



---

## **Total Evidence Phylogenetic Analysis Supports New Morphological Synapomorphies for Bovidae (Mammalia, Artiodactyla)**

Author: Calamari, Zachary T.

Source: American Museum Novitates, 2021(3970) : 1-38

Published By: American Museum of Natural History

URL: <https://doi.org/10.1206/3970.1>

---

BioOne Complete (complete.BioOne.org) is a full-text database of 200 subscribed and open-access titles in the biological, ecological, and environmental sciences published by nonprofit societies, associations, museums, institutions, and presses.

## Total Evidence Phylogenetic Analysis Supports New Morphological Synapomorphies for Bovidae (Mammalia, Artiodactyla)

ZACHARY T. CALAMARI<sup>1</sup>

### ABSTRACT

Advances in gene sequencing technology have made it easier to generate large molecular datasets with novel DNA sequences for phylogenetic analysis. Because morphological data are difficult to collect and not required for molecular phylogenetic analyses, they are often excluded in studies of the systematic relationships of extant taxa. This fact is especially apparent in the Bovidae, the highly diverse, widespread clade of hoofed mammals most often characterized by the presence of permanent bony horn cores covered with keratin sheaths. Analyses of molecular data have reconstructed well-supported phylogenetic relationships within the clade. However, morphological data are also required to integrate fossil taxa into these studies, and may support different topologies when they are included in total evidence phylogenies. In this study, I performed a maximum likelihood phylogenetic analysis of a total evidence dataset including mitochondrial genomes, nine nuclear genes, and 196 morphological characters. The dataset comprises 156 species, 13 of which are fossil taxa, one of the most complete analyses of the family to date, and the first time many of the fossil species have been included in a total evidence analysis. Character optimizations on this topology produced seven synapomorphic morphological characters for Bovidae and multiple characters for each tribe. These analyses support the use of total evidence phylogenetics as a means of uncovering morphological characters that may serve as new synapomorphies and elucidate the systematic relationships of fossil species.

---

<sup>1</sup> Department of Natural Sciences, Baruch College, City University of New York.

## INTRODUCTION

With advances in molecular sequencing technology have come innovations in molecular systematics. These new sequencing methods have extended molecular phylogenetic analyses beyond studies of only living taxa to include extinct taxa using ancient DNA. Analyses of both living and extinct species have helped elucidate relationships of species and clades historically difficult to place with morphological data alone (e.g., Troy et al., 2001; Decker et al., 2009; Delsuc et al., 2016; West, 2016). However, the rate at which DNA decays constrains the age of taxa we can study with ancient DNA; most methods can obtain reliable sequences from only the best-preserved samples of species that lived within the past 700,000 years (Hagelberg et al., 2015). Accordingly, morphological characters remain the only data available for many fossil taxa, and are essential for conducting phylogenetic analyses with these species. But to probe the deepest relationships on the tree of life, we need methods that combine molecular and morphological data in the reconstruction of phylogenies of extant and extinct taxa (de Queiroz et al., 1995; de Queiroz and Gatesy, 2007; Berger et al., 2011; Barbera et al., 2019), and for that we need to leverage not only the abundant characters available with molecular data but also the rich morphological data of the fossil record.

Bovidae is a diverse family within the ruminant even-toed hoofed mammals, or Ruminantia (Mammalia, Artiodactyla), that first appears in the Miocene, approximately 16–20 million years ago. Many of the extant tribes of Bovidae diverged within the past 10 million years (Bibi, 2013). The presence of permanent bony horn cores covered in a keratin sheath is an important character used to recognize both extinct and extant species as bovids (Gray, 1821; Janis and Scott, 1987; Bibi et al., 2009; DeMiguel et al., 2014); however, hornless taxa that could be early bovids are difficult to place confidently within phylogenies. Non-horn-core-based morphological characters offer complex and often contradictory evidence for bovid relationships, likely due to homoplasy resulting from the rapid diversification of bovids into ecosystems around the world (Bibi et al., 2009). Phylogenies based on molecular evidence often conflict with these morphology-based trees, especially in the systematic relationships and even monophyly of the different bovid tribes and genera (e.g., Gatesy et al., 1992; Gentry, 1992; Vrba et al., 1994; Gatesy and Arctander, 2000; Hassanin et al., 2012; Bibi, 2014). Likewise, different types of molecular evidence can produce conflicting results. Analyses of mitochondrial genomes alone have found multiple genera that are not monophyletic, for example, *Bos*, *Bison*, and *Capra* (Hassanin et al., 2012; Bibi, 2013); however, nuclear data (and morphological data) support their monophyly (Bibi, 2013). Whereas some genera have been united by morphological similarity, molecular evidence strongly supports their nonmonophyly, such as *Hemitragus*, now considered one of three separate genera alongside *Arabitragus* and *Nilgiritragus* (Ropiquet and Hassanin, 2005; Ropiquet, 2017), and *Neotragus*, which may be two genera instead of one (Bärmann and Schikora, 2014). Beyond questions of monophyly, several species have defied attempts to place them on a consistent branch in the bovid phylogeny, notably *Pelea capreolus*, *Pantholops hodgsonii*, *Saiga tatarica*, and *Aepyceros melampus* (Gatesy et al., 1992; Fernández and Vrba, 2005; Bibi, 2013, 2014; Robinson et al., 2014). Large-scale analyses of nuclear and mitochondrial genomes align *P. capreolus* with Reduncini, *P. hodgsonii* with Caprini, *S. tatarica*

with Antilopini, and *A. melampus* as sister taxon to Neotragini (Hassanin et al., 2012; Bibi, 2013; Chen et al., 2019).

Because of the homoplasy in bovid morphological characters and the wealth of character data provided by gene sequences, recent efforts to study bovid systematics often favor molecular phylogenetic data to the exclusion of morphological data. While molecular studies have found well-supported relationships for extant taxa, thorough morphological studies are required to determine how fossil taxa too old to allow viable DNA recovery fit into the bovid family tree. Including more fossil taxa in phylogenetic analyses of Bovidae can also improve estimates of clade divergence dates and result in more complete inferences of phylogeography and other important aspects of clade history (Bibi, 2013; Cantalapiedra et al., 2014, 2015). Moreover, increasing taxa in phylogenetic analyses can shorten branch lengths, reveal characters that serve as synapomorphies for important clades, and provide better support for relationships (Hillis, 1996; Zwickl and Hillis, 2002; Hedtke et al., 2006; Streicher et al., 2016), a valuable endeavor in efforts to understand both how the bovid tribes relate to each other and whether any hornless fossil species belong to the clade. Understanding the evolution of a widespread and economically important clade such as Bovidae requires studying not just living taxa, but the extensive fossil record of these animals as well.

Using both molecular and morphological characters in the same analysis can provide better resolution in phylogenies, especially when molecular evidence for ambiguous relationships is compelling and morphological characters are homoplastic (Eernisse and Kluge, 1993; Dávalos et al., 2014). In this study, I integrated mitochondrial genomes and nuclear DNA sequence data with morphological characters spanning living and extinct species in one of the most complete phylogenetic analyses of Bovidae to date. I optimized morphological characters on this total evidence phylogeny with the goal of identifying novel hard-tissue synapomorphies for Bovidae and its tribes that may provide evidence supporting the relationships of fossil species to the family.

## MATERIALS AND METHODS

**MOLECULAR DATA:** Nine nuclear genes were selected based on the availability of sequence data for a broad selection of bovids: spectrin beta nonerythrocytic 1 (SPTBN1, table S1.1), kappa casein exon 4 (CSN3, table S1.2), protein kinase C iota (PRKCI, table S1.3), amelogenin X-linked (AMELX, table S1.4), thyroid stimulating hormone beta (TSHB, table S1.5), stem cell factor (SCF, table S1.6), signal transducer and activator of transcription 5A (STAT5A, table S1.7), thyroglobulin (TG, table S1.8), and tumor necrosis factor alpha (TNF, table S1.9; all supplemental tables available in the online supplement, <https://doi.org/10.5531/sd.sp.49>). There were 107 bovid species with sequence data available for at least one of these genes on GenBank. I also obtained sequences for at least one of these genes for domestic pigs (*Sus scrofa*), Reeves' muntjac (*Muntiacus reevesi*), red deer (*Cervus elaphus*), mule deer (*Odocoileus hemionus*), caribou (*Rangifer tarandus*), and roe deer (*Capreolus capreolus*) to serve as outgroups. When a species had multiple sequences for a single gene available on GenBank, all sequences were aligned using the local alignment MAFFT algorithm, L-INS-I (Katoh et al., 2002). The majority

consensus sequence for that species was then computed, ignoring gaps introduced in the alignment, in Geneious 10.2.3 (<https://geneious.com>). BLAST searches of consensus sequences were performed against the GenBank nonredundant nucleotide database (nt) to ensure that they still produced close matches to the original genes. The gene sequence for each species was aligned using the L-INS-I algorithm in MAFFT, and after separate alignment of each gene, the alignments were then combined into a single nuclear data matrix with 7,372 molecular characters.

Mitochondrial genomes are available for many ruminant species, and thus they were an important source of molecular characters for the bovids in this study. Complete mitochondrial genomes for 123 species, including all six outgroup species from the nuclear DNA matrix (table S1.10 in the online supplement, <https://doi.org/10.5531/sd.sp.49>) were retrieved. Ancient DNA mitochondrial genomes were included for the helmeted muskox (*Bootherium bombifrons*), the aurochs (*Bos primigenius*), and the steppe bison (*Bison priscus*). Because mitochondrial genomes are circular, but MAFFT can treat sequences only as linear during alignment, nine species' sequences were edited based on their GenBank annotations to start with tRNA-Phe, the starting point for all other sequences: *Bison bison*, *B. priscus*, *Bos grunniens*, *Bos indicus*, *Bos mutus*, *Bos javanicus*, *Bos primigenius*, *Bos taurus*, and *Syncerus caffer*. The global alignment algorithm of MAFFT, G-INS-I, was then applied to produce a mitochondrial genome alignment with 18,069 characters.

**MORPHOLOGICAL DATA:** The morphological data comprised 196 craniodental and postcranial characters coded for 88 taxa analyzed across four studies (Gentry, 1992; Thomas, 1994; Bärmann, 2013, 2014). These data include 13 fossil species from nine of the tribes of Bovidae (table S2 in the online supplement, <https://doi.org/10.5531/sd.sp.49>). Gentry (1992) analyzed fossil taxa separately from the extant matrix (with the exception of three extant species that appear in both matrices), and had several characters coded only for fossils; for this study this fossil matrix was combined with the extant matrix based on the character correspondences provided in the paper (Gentry, 1992). No character descriptions were available for characters 33–36 in the fossil matrix, thus they were not included in this analysis. Thomas (1994) included essentially the same set of characters from Gentry's (1992) matrix, with the addition of two characters. He also added the saola (*Pseudoryx nghetinhensis*), anoa (*Bubalus depressicornis*), and Sumatran serow (*Capricornis sumatraensis*), as well as two nonbovid outgroups, the Indian muntjac (*Muntiacus muntjak*) and the Siberian musk deer (*Moschus moschiferus*). Musk deer characters from Thomas' (1994) matrix were not included here, as the species was not represented in any other data partition in this study. Additional craniodental characters were incorporated from Bärmann's studies of bovids (2013; Morphobank Project 352) and the tribe Antilopini (2014). Behavioral and soft tissue characters from these analyses were also not included in the present study, because they are features not commonly preserved in the fossil record and thus would be unlikely candidates to provide support for the placement of fossil taxa in phylogenies. When character descriptions in the different matrices unambiguously referred to the same feature, the characters were combined, reordering codings or combining relevant states as needed. Character descriptions from each of these sources are included in appendix 1 with explanations of how states were modified to facilitate the

matrix combination where appropriate. Thirty-four of these morphological characters were also encoded for four cervids based on Marcot's (2004) ruminant matrix to serve as an outgroup comparison for morphological character optimizations. *Muntiacus reevesi* and *Odocoileus hemionus*, two cervids for which much of the molecular data was available, were encoded as chimeras based on the congeners *Muntiacus muntjak* (see Thomas, 1994; Marcot, 2004) and *Odocoileus virginianus* (see Marcot, 2004). A table describing which species are represented in each data partition is located in the online supplemental information 2, and all character encodings are available in the phylip matrix file (supplemental file S3) and table S4.6 (available online, <https://doi.org/10.5531/sd.sp.49>).

**MAXIMUM LIKELIHOOD TREE SEARCH:** To assess how different data partitions might support the final total evidence analysis, separate analyses of each matrix (morphological, nuclear DNA, mitochondrial DNA), as well as a combined nuclear and mitochondrial DNA matrix, were conducted. Each molecular dataset was partitioned into coding and noncoding regions, using by-codon partitions for each protein-coding gene. The best fitting model of molecular evolution available in RAxML, GTR with gamma rate heterogeneity (GTR+G) or GTR+G with a proportion of invariant sites (GTR+I+G), was then assessed using the greedy search algorithm and linked branch lengths in PartitionFinder (Lanfear et al., 2017) on the CIPRES science gateway. GTR+G was the best-fitting model for the nuclear data analysis, and GTR+I+G was the best-fitting model for the mtDNA, combined molecular, and total evidence analyses. Before running each tree inference in RAxML, the best-scoring rearrangement setting was assessed following the recommendations of the RAxML v.8 user manual (Stamatakis, 2014, 2016). To find the topology with the best likelihood score, 200 inferences were then run for each separate partition. One-thousand-replicate nonparametric bootstrap branch supports were computed and applied to the topology with the best likelihood score (Stamatakis, 2014, 2016). For the morphological matrix, the multistate gamma MK model of evolution with an ascertainment bias correction (Lewis, 2001) was used, and the same procedures for determining a rearrangement setting, obtaining the best topology, and calculating bootstrap support values were followed. RAxML does not accept polymorphic character states, and so any polymorphic characters in the morphological matrix were converted to missing before analysis.

Next, both morphological and molecular data were combined into a single total evidence matrix to estimate the total evidence phylogeny of Bovidae. This final matrix included 156 species. Analysis of the best rearrangement setting, identification of the most likely topology, and calculation of bootstrap support values were performed following the RAxML manual (Stamatakis, 2014, 2016) as was done for the analyses of the separate partitions. The same partitioning scheme for molecular data and model of molecular evolution from the analysis of the combined nuclear and mitochondrial matrix (GTR+I+G) was used with the addition of the MK model with ascertainment bias correction (Lewis, 2001) for the morphological characters. Bootstrap support values were calculated and applied to the most likely topology following the same procedures as in all other analyses. The final total evidence matrix in phylip format can be found in file S3 (available at <https://doi.org/10.5531/sd.sp.49>). To assess the effects of missing morphological data on the ability to estimate fossil relationships, a total evidence phylogeny

was also computed for the 88 species represented in the morphological matrix using the same models of molecular and morphological evolution as the full total evidence analysis.

**BAYESIAN TREE SEARCH:** A time-calibrated Bayesian phylogeny was computed to examine potential differences in topology introduced by the choice of phylogenetic estimation method. Rather than combine partitions under the scheme assessed for the maximum likelihood analysis, all partitions were allowed to have separately-estimated models of molecular evolution, averaging across all reversible models available in the bModelTest package for BEAST2; all default priors were used for these models (Bouckaert and Drummond, 2017). When a single model is not strongly favored over others, averaging over all models rather than selecting a single model for each partition can account for the uncertainty (Bouckaert and Drummond, 2017).

Age ranges from Paleobiology Database (paleobiodb.org) provided the calibration times for all fossil species except *Sivatragus bohlini*, *Tragelaphus* sp., and *Turcoceros grangeri* (table 1). *S. bohlini* is Pliocene in age, according to Gentry (1992), thus I used the Pliocene stratigraphic age range (5.333–2.58 million years) from the International Chronostratigraphic Chart v 2020/03 (Cohen et al., 2013). For *Tragelaphus* sp., I used an age of 5.72 million years, based on Bibi (2013), and for *T. grangeri*, from the Tunggur Formation (Geraads, 2003), I used a range of 13–11.8 million years based on the age range of the formation as estimated from paleomagnetic correlations (Xiaoming et al., 2003). I used the fossilized birth-death process to model speciation, estimating all parameters except  $\rho$  (rho), the probability that an extant species would be sampled, which I fixed to 1 (Heath et al., 2014; Barido-Sottani et al., 2018). As the starting age for estimating the origin of Bovidae, I used a uniform distribution of  $58.6 \pm 3.2$  million years, based on the uniform dating model age with hard fossil calibration points estimated in a large-scale mitochondrial phylogeny of Artiodactyla (Hassanin et al., 2012).

**ANCESTRAL CHARACTER ESTIMATION:** Finally, to determine which characters map as synapomorphies for Bovidae or for clades within Bovidae, marginal ancestral state reconstructions were performed for each morphological character using RAXML-NG (Kozlov et al., 2019). Character 118 was excluded from the ancestral state reconstructions because it had either the same state encoded for all taxa or was polymorphic and marked as missing for analysis in RAXML, and thus could not be optimized in RAXML-NG. State changes were estimated on the most likely total evidence topology with the multistate MK model and correcting for ascertainment bias as in the morphological partition tree search. I then examined the best-supported character states from these analyses for state transitions at the nodes for Bovidae, the subfamilies Bovinae and Antilopinae, and the tribes as identified previous large-scale artiodactyl phylogeny using mitochondrial DNA (Hassanin et al., 2012). Because the total evidence analysis placed some fossil taxa in clades outside the tribes to which they most likely belong, I performed a second ancestral state reconstruction with these misplaced fossil species pruned from the phylogeny. I compared both ancestral state reconstructions to the characters coded for the fossil species to assess whether the synapomorphies would support their inclusion in those tribes, even if they were not correctly placed during the phylogenetic analysis.

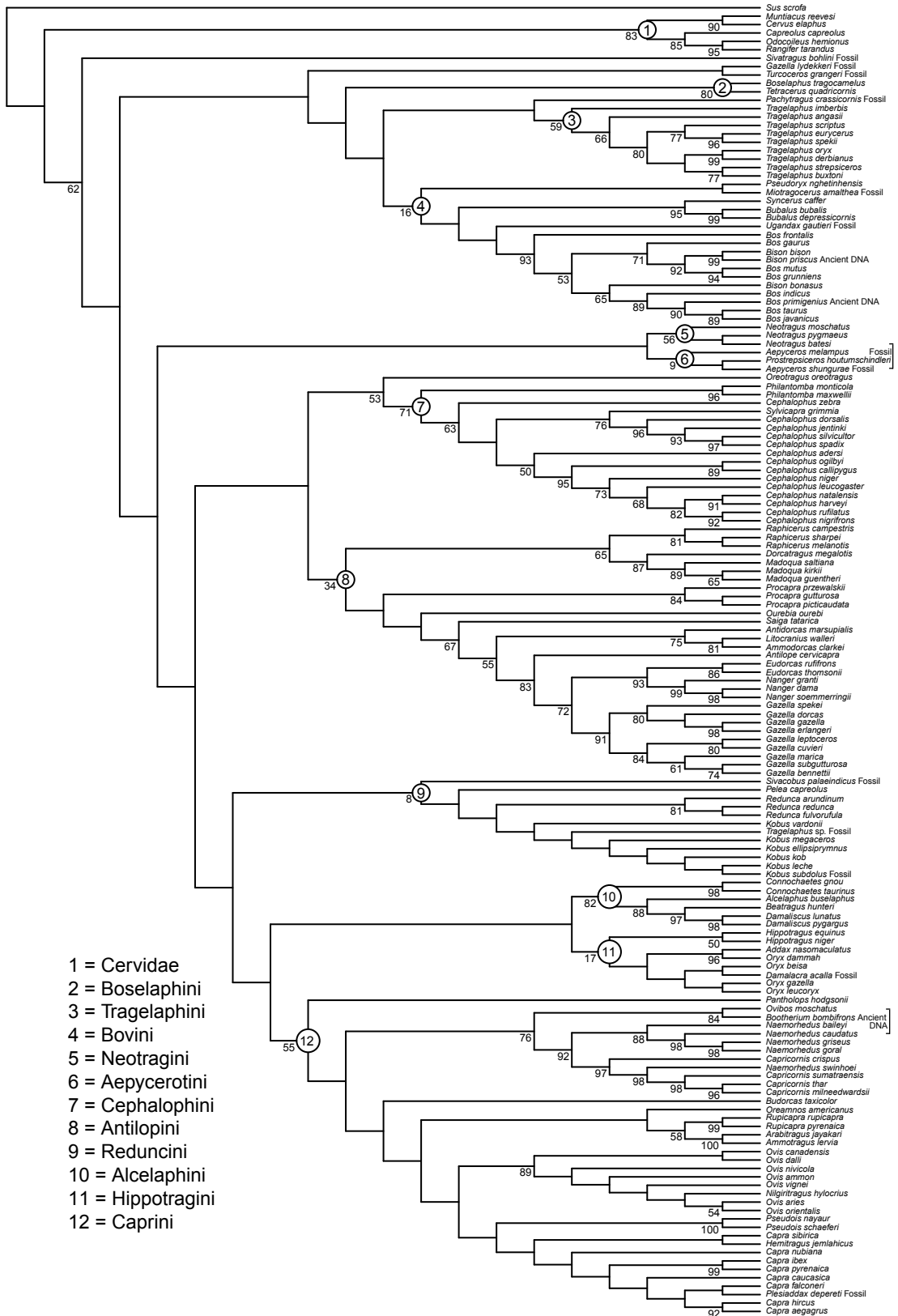
TABLE 1. Bayesian analysis fossil calibrations.

Fossil	Age (Ma)	References
<i>Aepyceros shungurae</i>	3.6–1.806	Paleobiology Database (PBDB)
<i>Bison priscus</i>	1.8–0.0117	PBDB
<i>Bootherium bombifrons</i>	1.8–0.0117	PBDB
<i>Bos primigenius</i>	2.588–0	PBDB
<i>Damalacra acalla</i>	5.333–3.6	PBDB
<i>Gazella lydekkeri</i>	15.97–3.6	PBDB
<i>Kobus subdolos</i>	5.333–3.6	PBDB
<i>Miotragocerus amalthea</i>	8.7–7.75	PBDB
<i>Pachytragus crassicornis</i>	11.608–5.333	PBDB
<i>Plesiaddax depereti</i>	11.608–5.333	PBDB
<i>Prostrepsiceros houtumschindleri</i>	11.608–8.7	PBDB
<i>Sivacobus palaeindicus</i>	0.781–0.0117	PBDB
<i>Sivatragus bohlini</i>	5.333–2.58	Gentry, 1992; Cohen et al., 2013
<i>Tragelaphus</i> sp.	5.72	Bibi, 2013
<i>Turcoceros grangeri</i>	13–11.8	Geraads, 2003; Xiaoming et al., 2003
<i>Ugandax gautieri</i>	11.62–3.6	PBDB

## RESULTS

### TOPOLOGY

The most likely topology from the maximum likelihood total evidence analysis recovered monophyletic tribes of extant bovids; however, support for most tribes and internal nodes was below 75% (fig. 1). Hippotragini, Reduncini, Antilopini, Aepycerotini, and Bovini all had bootstrap support well below 50%. Caprini, Neotragini, and Tragelaphini had bootstrap supports of 55%, 56%, and 59%, respectively. The node describing the bifurcation between the single representative of Oreotragini in this analysis and the Cephalophini received similarly moderate support (53%). Cephalophini (71%) and Alcelaphini (82%) had relatively strong bootstrap support values. Most of the nodes describing relationships between the tribes and other deeper relationships (i.e., nodes for the subfamilies Bovinae and Antilopinae) also had low bootstrap support, while the highest levels of support were generally for nodes toward the tips. Only four of the 13 fossil species in the morphological data matrix aligned with their most likely tribes (table 2). *Sivacobus palaeindicus*, *Miotragocerus amalthea*, and *Damalacra acalla* placed as sister taxa to their most likely tribes. *Sivatragus bohlini*, although placed outside the tribe where it would be expected (Hippotragini), had the highest support for a fossil species based only on morphological data (62%), while the three species represented by ancient DNA mitochondrial genomes had strong support (84% *Ovibos moschatus* and *Bootherium bombifrons*, 99% for *Bison priscus*). The



total evidence analysis of the 88 species for which morphological data were available resulted in the same relationships for fossil species as the full, 156 species analysis, thus only the phylogenies with more complete taxon sampling were considered for character optimizations.

Several genera were not monophyletic on the total evidence phylogeny. *Bison* and *Bos* were not reciprocally monophyletic. The American bison (*Bison bison*) and the steppe bison (*B. priscus*) were each other's closest relatives, but linked to the sister taxa wild and domestic yaks (*Bos mutus* and *Bos grunniens*). Bootstrap support for this relationship was 92%. The gaur (*Bos gaurus*) was the sister taxon to this four-species clade, with 71% bootstrap support. The European bison (*Bison bonasus*) was sister taxon to a clade containing most of the rest of the species of *Bos* (except for the gayal, *Bos frontalis*), with 65% bootstrap support. In the Antilopinae, *Sylvicapra grimmia* nested within the genus *Cephalophus*, with moderate support (76%). *Addax nasomaculatus* as sister taxon to *Oryx dammah* had strong support (96%), but only in the analyses that included mitochondrial genomes; *A. nasomaculatus* only had mitochondrial DNA and morphological data in these analyses. *Naemorhedus swinhoei* nested within *Capricornis*, instead of with the other species from *Naemorhedus*, with strong support (98%). *Nilgiritragus hylocrius* was sister taxon to *Ovis aries* and *Ovis orientalis*, disrupting the monophyly of *Ovis*; however, this position was essentially unsupported at 32% bootstrap support. The total evidence analysis also placed *Hemitragus jemlahicus* within *Capra*, with similarly low support (33%). These genera also were not monophyletic on the most likely nuclear-DNA-only topology (fig. 2), with the exception of *Oryx*, which had data for fewer species and no data for *A. nasomaculatus* in the matrix.

The analyses of separate data partitions had different patterns of support, usually across the whole tree. The most likely topology for the morphological data showed very little support above the genus level; most internal nodes had no bootstrap support (fig. 3). This morphological topology resolved few of the tribes as monophyletic. The species of Reduncini were in a monophyletic group, with low bootstrap support, and the Cephalophini were monophyletic with moderate support. The Alcelaphini and Hippotragini were combined into a single group of species with low support, and the Caprini nested within the Antilopini. Fossils were generally misplaced with respect to other species of their likely tribes. *Kobus subdolanus* maintained a sister taxon relationship with *Kobus leche*, and *Sivacobus palaeindicus* nested within the genus *Kobus*, albeit with low bootstrap support, rather than outside Reduncini + *Pelea* as it did in the total evidence phylogeny. *Ugandax gautieri* did not form a clade with other species of Bovini, and *Aepyceros shunguruae* was not sister taxon to *Aepyceros melampus*. *Turcoceros grangeri* was sister taxon to *Antilope cervicapra* at the base of a clade containing species of both Antilopini and Caprini, closer to its likely tribe (Caprini), than it was on the total evidence topology. *Miotragoceros amalthea* in the morphological analysis was sister taxon to *Tragelaphus scriptus*; there was neither a monophyletic Tragelaphini nor a monophyletic Boselaphini on this topology.



FIGURE 1. Total evidence maximum likelihood topology of Bovidae. Node labels are bootstrap supports over 50 and extinct species are labeled Ancient DNA or Fossil to denote how they appear in the matrix. Bootstrap values for tribes are displayed regardless of support level.

TABLE 2. Fossil species and tribes. Comparison of the most likely tribal affinity for each fossil species to its placement in the maximum likelihood total evidence phylogeny.

Species	Most likely	Total Evidence
<i>Aepyceros shunguræ</i>	Aepycerotini	Aepycerotini
<i>Damalacra acalla</i>	Alcelaphini	Hippotragini
<i>Gazella lydekkeri</i>	Antilopini	–
<i>Prostrepsiceros houtumschindleri</i>	Antilopini	Aepycerotini
<i>Miotragocerus amalthea</i>	Boselaphini	Bovini
<i>Ugandax gautieri</i>	Bovini	Bovini
<i>Pachytragus crassicornis</i>	Caprini	–
<i>Plesiaddax depereti</i>	Caprini (Ovibovina)	Caprini
<i>Turcoceros grangeri</i>	Caprini	–
<i>Sivatragus bohlini</i>	Hippotragini	–
<i>Kobus subdolos</i>	Reduncini	Reduncini
<i>Sivacobus palaeindicus</i>	Reduncini	Reduncini*
<i>Tragelaphus</i> sp. (Gentry 1992)	Tragelaphini	Reduncini

\**S. palaeindicus* was located as the sister taxon to *Pelea* + Reduncini, potentially accurate if *Pelea* is considered a true reduncine.

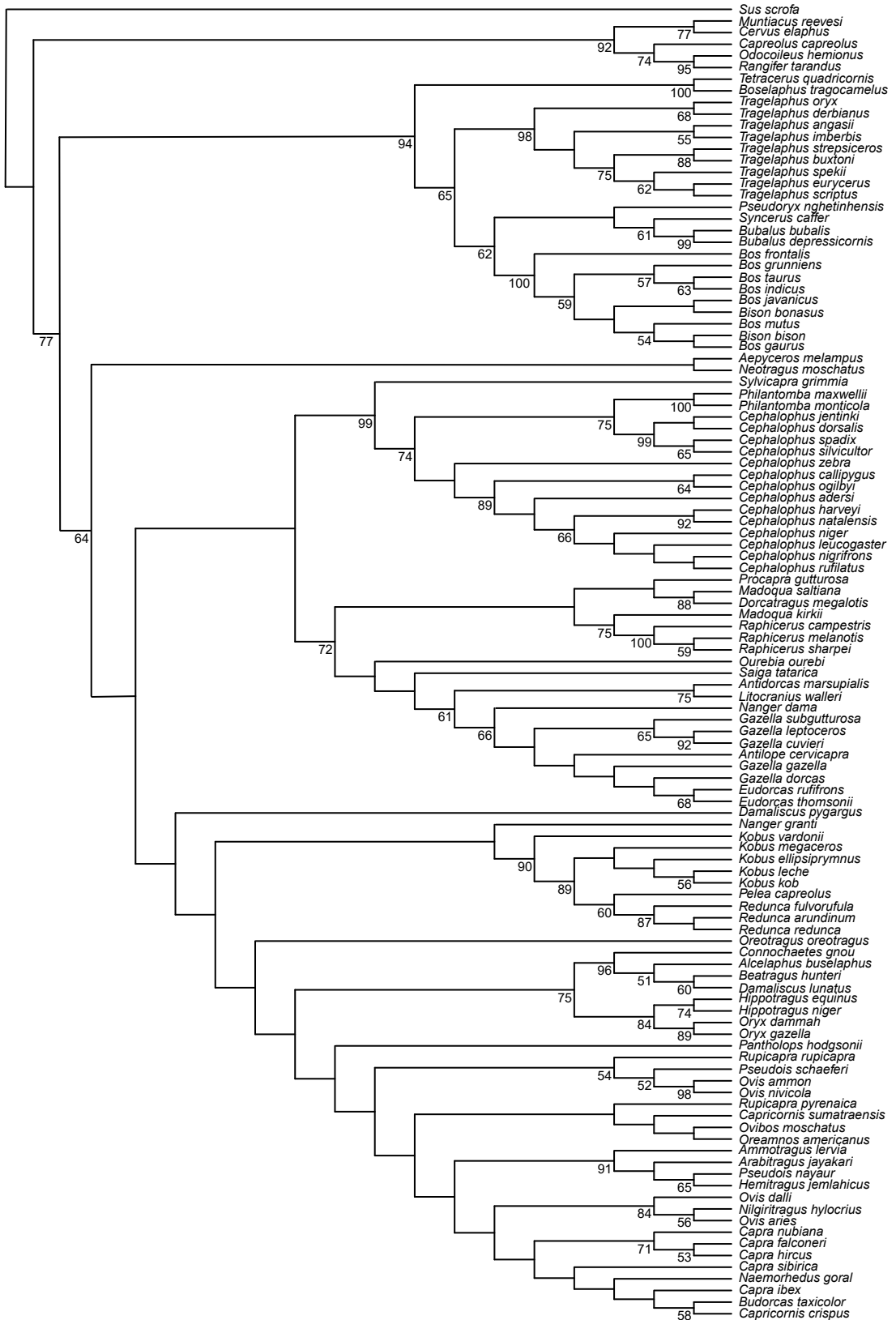
In the separate molecular data analyses, tree structure was fairly similar, and most tribes were monophyletic. All tribes of the subfamily Bovinae were monophyletic in the molecular data partitions. However, the nuclear data (fig. 2) resolved *Pseudoryx nghetinhensis*, the saola, as the sister taxon to Bubalina (the subtribe of water buffalo and African buffalo), while the mitochondrial data (fig. 4) placed it as sister taxon to all other species of Bovini. Nuclear data did not support a monophyletic *Cephalophus*, while mitochondrial DNA did, but placed *Sylvicapra grimmia* within the genus. Similarly, the nuclear DNA data did not support monophyly for *Madoqua*, *Gazella*, *Nanger* (*Nanger granti*, in particular, was grouped with Reduncini) in Antilopini, *Damaliscus* in Alcelaphini, nor *Capra*, *Rupicapra*, and *Ovis* in Caprini. Neither the nuclear nor the mitochondrial data recovered a monophyletic *Bison*. The mitochondrial phylogeny placed *A. nasomaculatus* within the genus *Oryx*, as in the total evidence analysis, but this placement could not be compared with the nuclear data analysis because *A. nasomaculatus* had no nuclear data represented in that matrix. Similar to the total evidence analysis, *Naemorhedus swinhoei* was located in the genus *Capricornis* in the mitochondrial DNA analysis. Relationships between tribes were generally similar in both the nuclear and mitochondrial analyses, except for the position of *Oreotragus*. It was sister taxon to Caprini + Hippotragini + Alcelaphini in the nuclear analysis, but sister taxon to Cephalophini in the mitochondrial analysis. The analysis of both molecular partitions as a single supermatrix (fig. 5) resulted in a topology that was nearly identical to the mitochondrial topology, differing only in the addition of species not represented in the mitochondrial matrix. This analysis placed *Kobus vardonii* as sister taxon to *Pelea* + Reduncini, with 94% bootstrap support.

In the dated Bayesian total evidence analysis (fig. 6), the major relationships between the tribes were unchanged from the maximum likelihood analysis. In most cases, fossil species were located well outside of their expected positions, with eight placing outside crown Bovidae entirely. Of the species that were located within extant tribes, *M. amalthea*, *U. gautieri*, and *S. palaeindicus* placed within their expected tribes, and *D. acalla* was located in Hippotragini instead of Alcelaphini, as in the maximum likelihood tree. *S. bohlini* was placed as the sister taxon to Neotragini in this topology, far outside the expected relationship to Hippotragini. As with the maximum likelihood phylogeny, support values were low, especially for the deepest relationships on the tree. Because this Bayesian analysis resulted in particularly unreasonable placements for the fossil taxa but otherwise produced the same topology for the extant tribes as estimated in the maximum likelihood analysis, it was not used for character optimizations.

#### SYNAPOMORPHIES

Ancestral state reconstructions on both the total evidence topology (referred to as the full topology) and the topology with fossils located outside their likely tribes pruned (referred to as the reduced topology) produced a large number of characters that mapped as synapomorphies for tribes, subfamilies, and Bovidae (tables S4.1–4.6 in the supplement, available at <https://doi.org/10.5531/sd.sp.49>). For the purpose of identifying characters that can link fossils to their most likely tribes within Bovidae, fossil comparisons were made for any character that met four criteria: the character mapped as a synapomorphy for that tribe (i.e., characters with a reconstructed state for the common ancestral node of a tribe that differed from the node immediately preceding it), it was coded for more than one species in the tribe, it had the same character state as most of those species, and it differed from the character state reconstructed for Cervidae (table 3). Not considered were characters that mapped as synapomorphies for *Oreotragus oreotragus*, as it was the only member of its tribe represented in this matrix, and thus its synapomorphies were indistinguishable from autapomorphies for that species. A larger number of characters mapped as synapomorphies on the reduced topology, but many of these characters were based on a single taxon or were not representative enough of the majority of the tribe to aid in the identification of phylogenetic affinities of the fossils. The majority of characters that met the criteria for inclusion mapped as synapomorphies on both the full and reduced topology (table S4.5).

*Aepyceros shungurae* had three characters in common with the proposed synapomorphies from Aepycerotini: long horn cores (char. 1, state 2), presence of a postcornual fossa (char. 12, state 1), and the presence of a transverse metaconid ridge on p3 (char. 55, state 1) (Gentry, 1992; Thomas, 1994). *Gazella lydekkeri* similarly had only one character that matched the synapomorphies of Antilopini: the position of the external auditory meatus' opening in lateral view is at or above the mandibular fossa (char. 184, state 1) (Bärmann, 2013, 2014). Two other characters could support inclusion of *G. lydekkeri* in Antilopini, a posterolingual cristid fusing the metaconid and entoconid on p4 (char. 133, state 1) and lack of contact between the nasal and lacrimal bones (char. 151, state 0), but these characters were



also synapomorphies for Cephalophini and Hippotragini, respectively. *Pachytragus crassicornis* and *Plesiaddax depereti* both shared the presence of a flattened lateral surface of the horn core (char. 112, state 0) (Gentry, 1992) and mediolaterally compressed horn cores as a synapomorphy of Caprini (char. 196, state 1) (Gentry, 1992; Thomas, 1994; Bärmann, 2013, 2014). *P. depereti* also shared an indistinct paraconid on p3 and p4 (char. 56, state 0) (Gentry, 1992; Thomas, 1994; Bärmann, 2013, 2014) with Caprini, but this character also mapped as a synapomorphy for Cephalophini and Neotragini. Two characters matched between *T. grangeri* and the synapomorphies for Caprini: a roughly triangular-shaped tympanic bulla in lateral view (char. 179, state 1) and laterally directed opening of the external auditory meatus in ventral view (char. 183, state 0) (Bärmann, 2013, 2014). Two synapomorphies for Caprini that matched with *T. grangeri*, a third lobe of m3 consisting only of a hypoconulid (char. 137, state 2) and horn cores that diverge in frontal view (char. 193, state 1) (Bärmann, 2013, 2014), also mapped as synapomorphies for Boselaphini and Reduncini, respectively. *Ugandax gautieri* matched the synapomorphies for Bovini with just the presence of horn cores that are notably inclined in lateral view (char. 6, state 1) (Gentry, 1992; Thomas, 1994). *Kobus subdolosus* and *Sivacobus palaeindicus* both have the reduncine synapomorphy of a braincase that is approximately the same width along the anteroposterior axis (char. 109, state 1) (Gentry, 1992). No characters mapped as a synapomorphy and met the inclusion criteria for Tragelaphini, and no other fossil species shared synapomorphies from either topology with their tribes.

Characters that mapped as synapomorphies for Bovidae on the full topology fit the criteria for inclusion better than those from the reduced topology. Many character reconstructions from the reduced topology that mapped as synapomorphies were based on few coded species and did not match with observed character states, and so were not considered in these fossil comparisons. In addition, the synapomorphic characters for Bovidae on the full topology were all coded for the cervid outgroups, lending more credence to their value for identifying fossils as bovids. Seven characters mapped as synapomorphies for Bovidae on the full topology, including three that matched to both *G. lydekkeri* and *T. grangeri* and two that matched to only *G. lydekkeri* among the fossil species. The three bovid synapomorphies found in *G. lydekkeri* and *T. grangeri* were a P2 of equivalent size to P3 (char. 119, state 2), a gap between the nasal and maxilla bones (char. 150, state 0), and horn cores that are centered on a point above the posterior margin of the orbit in lateral view (char. 187, state 0) (Bärmann, 2013, 2014). *G. lydekkeri* also had mesodont molars (based on the hypsodonty index of m3; char. 138, state 1), and a tympanic bulla that is inflated to the level of the occipital condyles (char. 176, state 1) (Bärmann, 2013, 2014). No fossil species had character 45, state 1, intermediate-sized foramina ovalia (Gentry, 1992; Thomas, 1994; Bärmann, 2013, 2014), or character 154, state 1, presence of only one lacrimal foramen on each side of the cranium (Bärmann, 2013, 2014), the last two bovid synapomorphies identified in this analysis.



FIGURE 2. Nuclear DNA maximum likelihood topology. Node labels are bootstrap supports over 50.



FIGURE 3. Morphological data maximum likelihood topology. Node labels are bootstrap supports over 50. Extinct species are labeled Fossil.

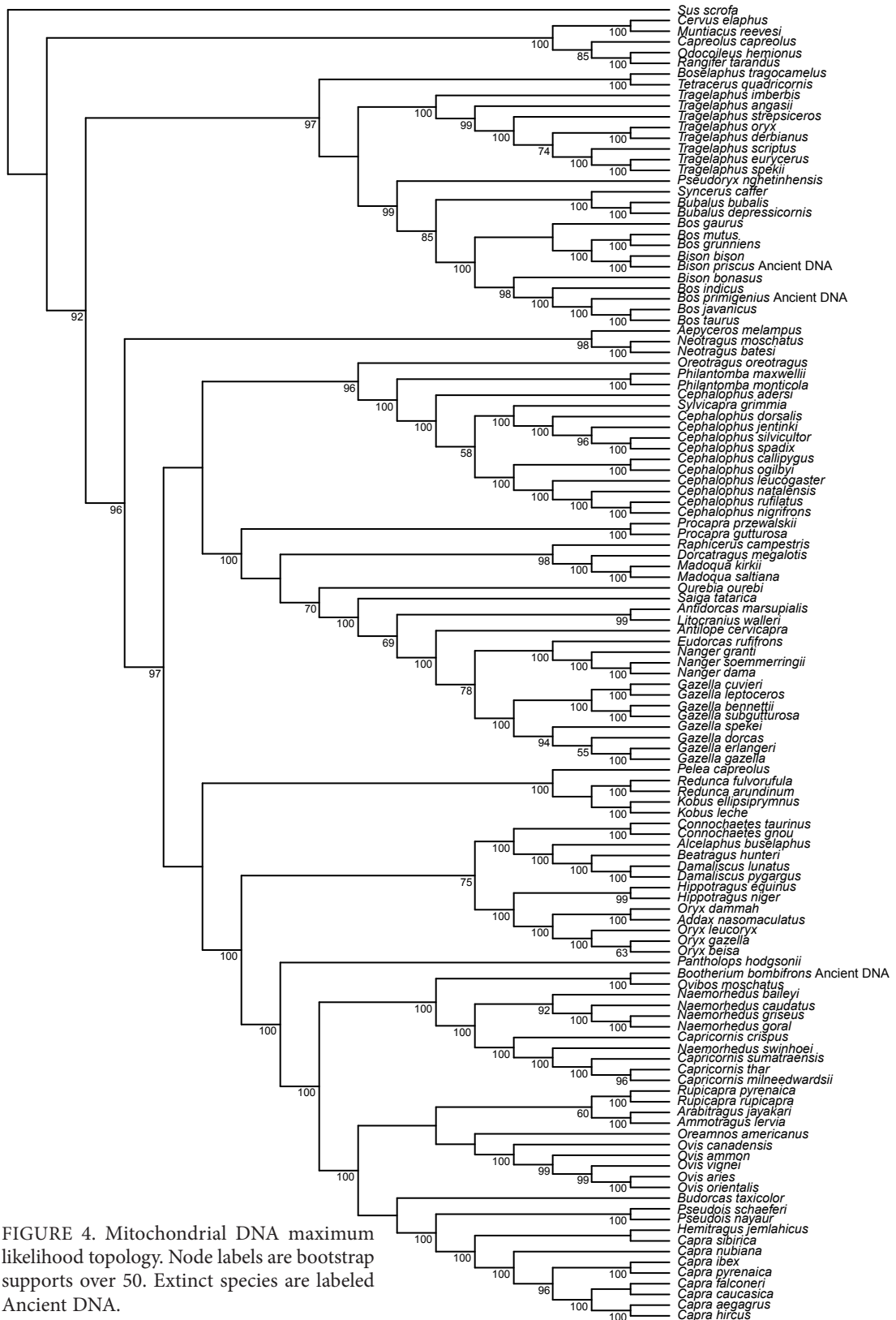


FIGURE 4. Mitochondrial DNA maximum likelihood topology. Node labels are bootstrap supports over 50. Extinct species are labeled Ancient DNA.

TABLE 3. Synapomorphic characters for Bovidae and its tribes.

Tribe	Synapomorphic Character: Character State
Aepycerotini	1: 2, 12: 1*, 55: 1
Alcelaphini	38: 1, 125: 1, 129: 0**, 132: 1, 139: 2, 143: 2, 144: 2, 155: 0*, 163: 2, 164: 3, 171: 0*, 188: 1**, 193: 2, 195: 2*
Antilopini	59: 1, 80: 1, 88: 1, 97: 1, 131: 1, 133: 1, 137: 3*, 151: 0, 172: 1, 184: 1
Boselaphini	5: 1, 14: 1, 83: 1, 101: 0**, 122: 1, 135: 1, 137: 2**, 158: 1, 172: 0*, 178: 1, 187: 1*, 188: 2*
Bovini	6: 1, 14: 1, 29: 1, 42: 1, 46: 1, 48: 0, 69: 0**
Caprini	14: 1*, 29: 1*, 45: 1, 51: 0, 53: 1*, 56: 0*, 63: 1, 93: 1, 112: 0**, 132: 1*, 137: 2**, 179: 1, 183: 0**, 193: 1**, 196: 1
Cephalophini	11: 2, 56: 0, 122: 1, 124: 2*, 126: 1, 133: 1, 137: 2**, 138: 1*, 148: 1, 150: 1, 155: 0, 160: 1, 164: 2, 165: 0, 187: 1*, 188: 1**, 194: 0**
Hippotragini	69: 0, 122: 2, 129: 0**, 134: 0**, 135: 1, 136: 1, 151: 0*, 172: 1*, 182: 0*, 189: 4, 194: 0**
Neotragini	56: 0, 134: 0*, 145: 1**, 153: 0*, 156: 1**, 169: 1**, 172: 0*, 174: 1*, 183: 1*, 188: 2*, 194: 0*
Reduncini	39: 0**, 69: 0, 109: 1**, 122: 1, 124: 2*, 125: 1, 135: 1, 136: 1, 140: 1*, 146: 4, 151: 0**, 165: 0*, 172: 0*, 180: 0*, 193: 1**, 195: 1**
Tragelaphini	—
Bovidae	45: 1, 119: 2*, 138: 1*, 150: 0*, 154: 1*, 176: 1*, 187: 0*

\*Only on the full topology; \*\* only on the reduced topology.

## DISCUSSION

### TOPOLOGY

Systematic positions of fossil species were generally poorly supported on the maximum likelihood total evidence topology, likely due to the lack of clear phylogenetic signal in the morphological data matrix. This discussion will focus on the maximum likelihood total evidence topology because it was used for morphological character optimizations. Of the four species that aligned with their most likely tribes, their positions within the tribes were not well supported. *Ugandax gautieri* often aligns with the African and water buffaloes (Bibi, 2007), while here it was the sister taxon to the *Bos* + *Bison* clade. *Plesiaddax depereti* likewise was located in the wrong subtribe of Caprini. Expected to align with Ovibovina (Gentry, 1992), it instead nested in Caprina in the genus *Capra*. In the Reduncini, *Kobus subdolos* was sister taxon to *Kobus leche*, and had the second-highest bootstrap support of the relationships within *Kobus* (although support was low throughout the genus), in contrast to other analyses that place *K. subdolos* in *Redunca* (Vrba, 2006; Vrba and Haile-Selassie, 2006).

Among the fossils placed outside, but near, their likely tribes, *Miotragocerus amalthea* offers a tantalizing hint for revising relationships within the subfamily Bovinae. Whether fossil boselaphines actually belong in the tribe is unclear (Bibi, 2007; Bibi et al., 2009); *M. amalthea* as the sister taxon to the bovine *Pseudoryx nghetinhensis*, the saola, had higher support relative to the other fossil species' placements (albeit still low at 16%). The saola itself is morphologically disparate compared with other bovines (Gatesy and Arctander, 2000), and

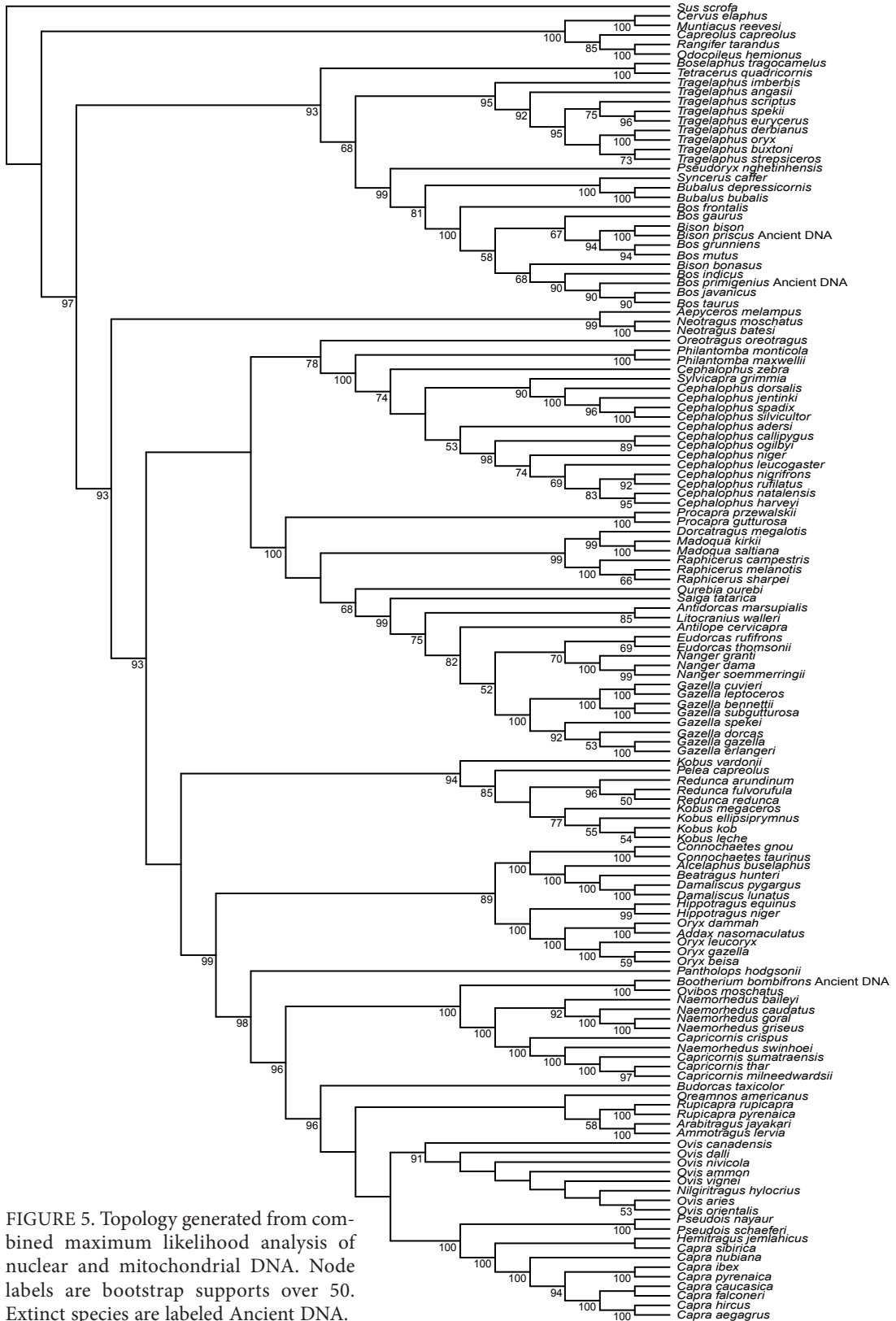


FIGURE 5. Topology generated from combined maximum likelihood analysis of nuclear and mitochondrial DNA. Node labels are bootstrap supports over 50. Extinct species are labeled Ancient DNA.

it is possible that the two are linked here because they are derived relative to other members of Bovinae. However, *M. amalthea* had more characters in common with *P. nghetinhensis* (12 of the 31 characters encoded for it) than with either living boselaphine or most other bovines. If the position of *M. amalthea* is robust to the addition of more morphological characters and more fossil boselaphines, it could help fill in the history of morphological changes that distinguish the enigmatic saola from other members of Bovini.

Of the nonmonophyletic genera on the total evidence topology, several are well documented to lack monophyly when analyzed with certain data. Lack of reciprocal monophyly for *Bison* and *Bos* on this total evidence phylogeny and each separate analysis of the molecular data is a common pattern in phylogenetic analyses. Multiple studies have found evidence for introgression among species of these two genera (Verkaar et al., 2004; Hassanin et al., 2013; Wu et al., 2018). Given the consistent lack of monophyly of *Bison* and *Bos* across multiple studies, it is clear that a thorough reassessment of these genera drawing on the many fossil species not included here and a larger set of morphological characters is required. Such an analysis could potentially support the inclusion of *Bison* as a junior synonym of *Bos*. *Sylvicapra* could also be considered a junior synonym of *Cephalophus*, and *S. grimmia* could be transferred to *Cephalophus*, given its well-supported placement within that genus on this phylogeny and in previous research (Hassanin et al., 2012; Johnston and Anthony, 2012; Bibi, 2013).

The relationship between *Oryx dammah* and *Addax nasomaculatus*, although strongly supported in this analysis, is contradicted by other studies (Bibi, 2013; Hassanin et al., 2013). Fertile hybrids between *O. dammah* and *A. nasomaculatus* are possible (Engel, 2004; Gilbert, 2017), which could support an interpretation that their pairing here is evidence for introgression captured in the molecular data. Monophyly for various clades within Caprini (the tribe containing *Capricornis*, *Naemorhedus*, *Ovis*, *Capra*, *Nilgiritragus*, and *Hemitragus*) has also been inconsistent in past studies (Hassanin et al., 1998, 2012). However, this total evidence topology has more nonmonophyletic genera than previous studies, which mostly agree on the placement of *H. jemlahicus* as sister taxon to *C. sibirica* (Hassanin et al., 1998, 2012; Bibi, 2013). Although previous research suggests that *Neotragus* is a polyphyletic genus (Bärmann and Schikora, 2014), the total evidence topology presented here does not support that interpretation; all three members of the genus form a single clade with moderate bootstrap support.

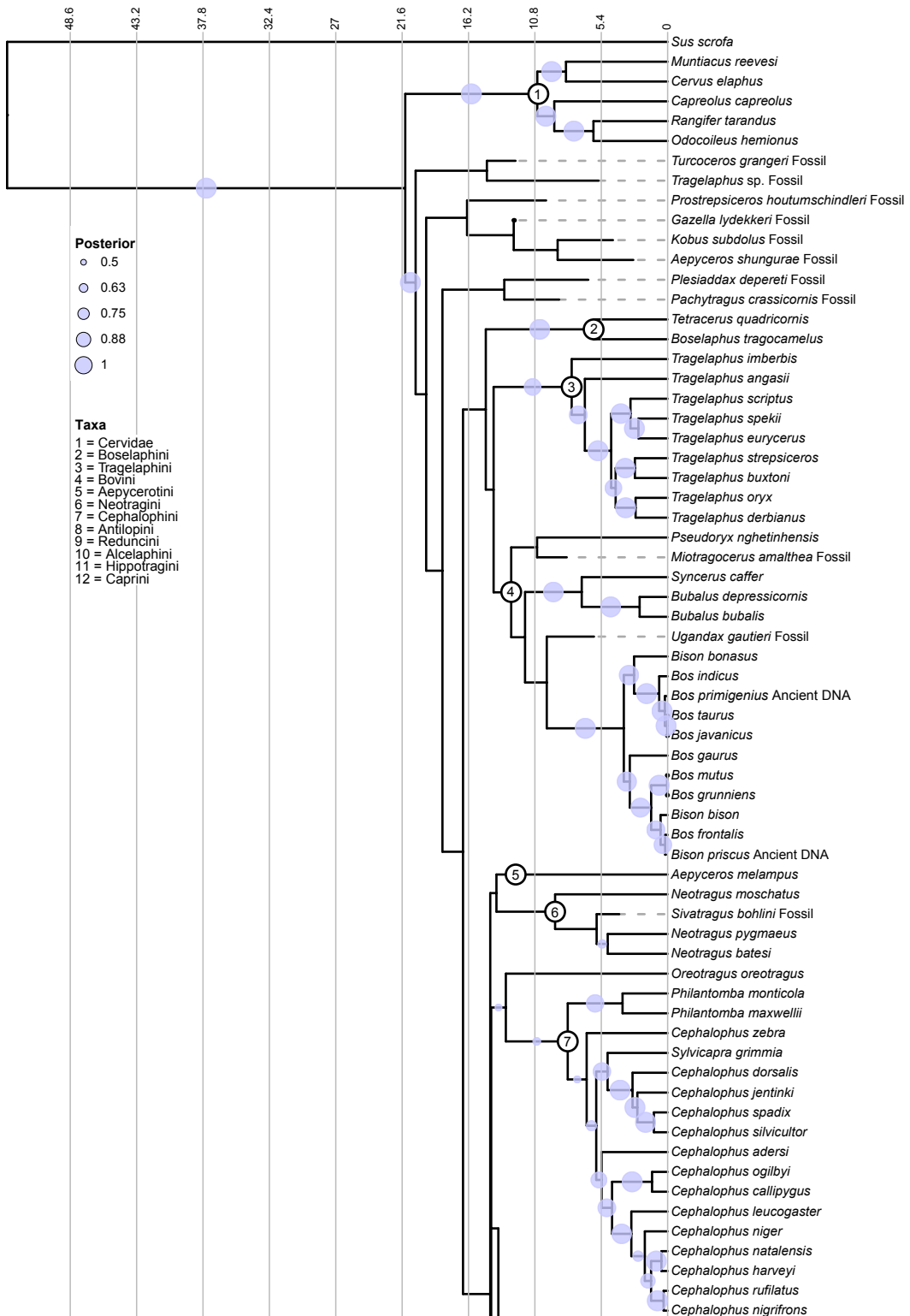
The relationships of tribes in Bovinae were similar in this analysis to previous molecular phylogenies: Tragelaphini and Bovini were sister taxa, with Boselaphini as the sister taxon of that pairing (Marcot, 2007; Decker et al., 2009; Hassanin et al., 2012; Chen et al., 2019). This grouping is contradicted in another analysis of combined morphological and molecular data with more limited taxonomic sampling (Gatesy and Arctander, 2000), as well as two of the morphological analyses that provided characters analyzed in this study (Gentry, 1992; Thomas, 1994), which group Bovini with Boselaphini as sister taxa instead. The extant species of Boselaphini are morphologically disparate, and their relationship to fossil boselaphine species is unclear (Bibi, 2007; Bibi et al., 2009). Although the analysis presented here agreed with the placement of Boselaphini as the sister taxon to the rest of Bovinae, including the other fossils

attributed to the tribe and subfamily and a more robust character set in future analyses may help determine which position for the tribe should be favored.

Tribal relationships within Antilopinae differ greatly in this analysis from those recovered by previous molecular and supermatrix studies. Previous analyses of molecular data supported a Hippotragini + Alcelaphini clade with Caprini as its sister taxon, similar to the one found in this total evidence topology (Marcot, 2007; Hassanin et al., 2012). The sister taxon to the Hippotragini + Alcelaphini + Caprini in a supermatrix analysis of nuclear and mitochondrial genes was Antilopini (Marcot, 2007), but an analysis of mitochondrial genomes alone placed Cephalophini + Oreotragini as the sister taxon to this clade (Hassanin et al., 2012). The total evidence analysis in this paper proposes yet another grouping of these tribes. The Hippotragini + Alcelaphini + Caprini clade is linked to Reduncini, as in Bibi's (2013) mitochondrial DNA analysis. Oreotragini + Cephalophini is the sister clade to Antilopini on the total evidence topology, which in turn is sister taxon to the clade containing Hippotragini, Alcelaphini, Caprini, and Reduncini. The position of Aepycerotini and Neotragini as a sister clade to the rest of the tribes in Antilopinae, however, is found in most recent large-scale molecular analyses and may simply be a case of two highly derived families clustering with each other (Hassanin et al., 2012; Bibi, 2013; Chen et al., 2019). Including fossil species from either tribe in a future analysis would be a good test of whether fossil species represented only by morphology in total evidence analyses can accomplish the increased taxon sampling required to break up long branches (Hillis, 1996) and support a different position for these families.

The similarities of the total evidence phylogeny to other maximum likelihood analyses of mitochondrial genomes or combined mitochondrial and nuclear data (e.g., Hassanin et al., 2012; Bibi, 2013; Bärermann et al., 2013) suggest that the mitochondrial genomes have a strong effect on topology, which may be unsurprising, given that they formed the largest partition in the total evidence matrix. The absence of mitochondrial data for several species, however, did not seem to preclude placing those species with the correct tribe or genus. Instead, the differences in the availability of nuclear data may have been more determinative. More nuclear genes were available for *Bison bonasus* than for *Bison bison*; half the species of *Bos* that grouped with *B. bonasus* had sequences for AMELX, while none of those that grouped with *B. bison* did. For the Cephalophini, *C. zebra* is represented in the matrix only by sequence data for TSHB, while *S. grimmia* and nearly all other species of *Cephalophus* also had PRKCI sequences and mitochondrial genomes. For the other nonmonophyletic genera, however, there were no clear patterns between species represented by different nuclear genes and the lack of monophyly.

The lack of morphological data does not appear responsible for the misplacement of species, as multiple extant species that were present only in the morphological matrix (e.g. *Neotragus pygmaeus*, *Procapra picticaudata*, *Gazella marica*) nonetheless joined their congeners in monophyletic groups, albeit with lower bootstrap support values. Low bootstrap support was likely related more to conflicting phylogenetic signal in the nuclear and mitochondrial data or the nearly complete lack of signal in the morphological data than to the presence of species with missing data. Missing data alone do not prevent accurate placement of species in a phylogeny when there are many characters in the matrix (Wiens, 2003; Wiens



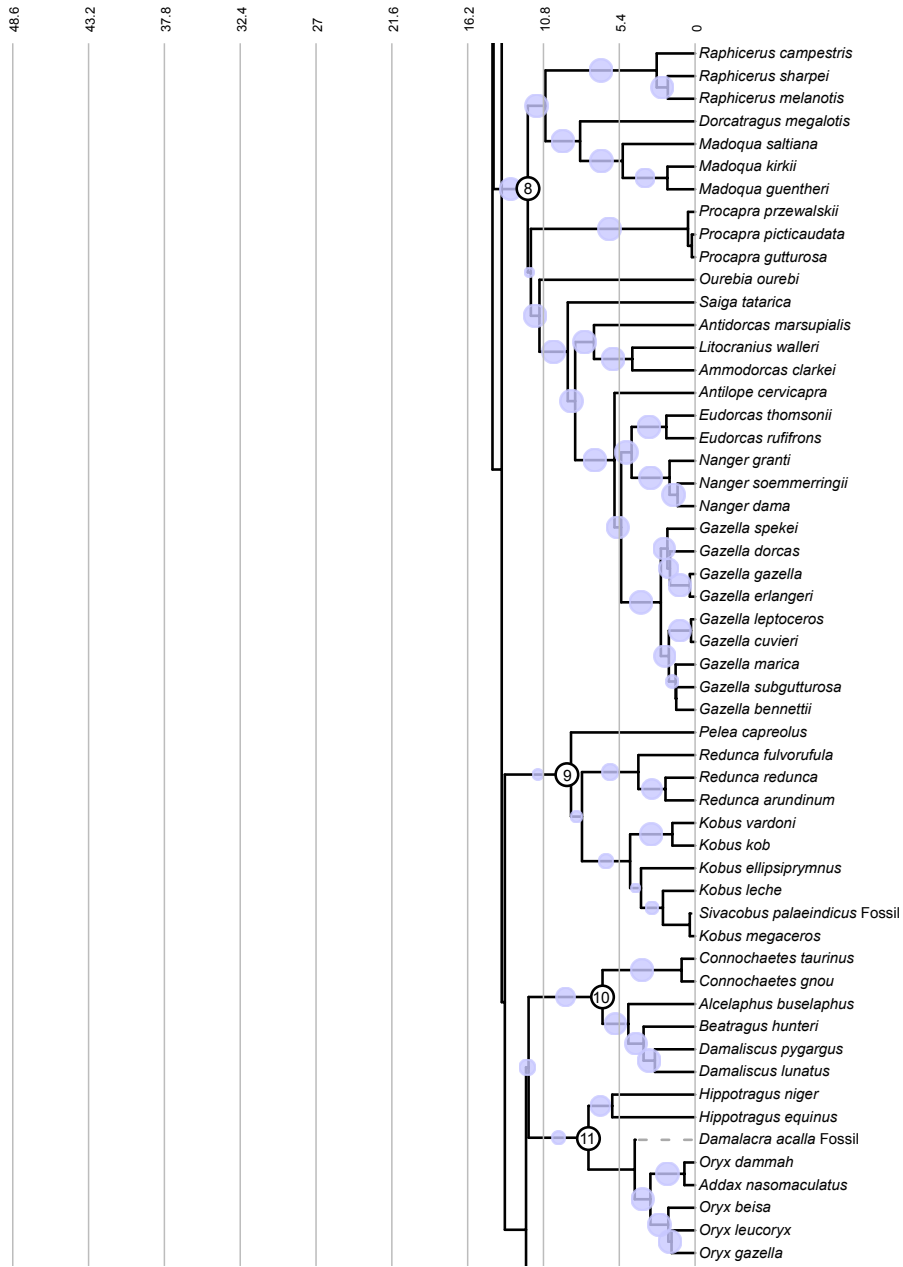
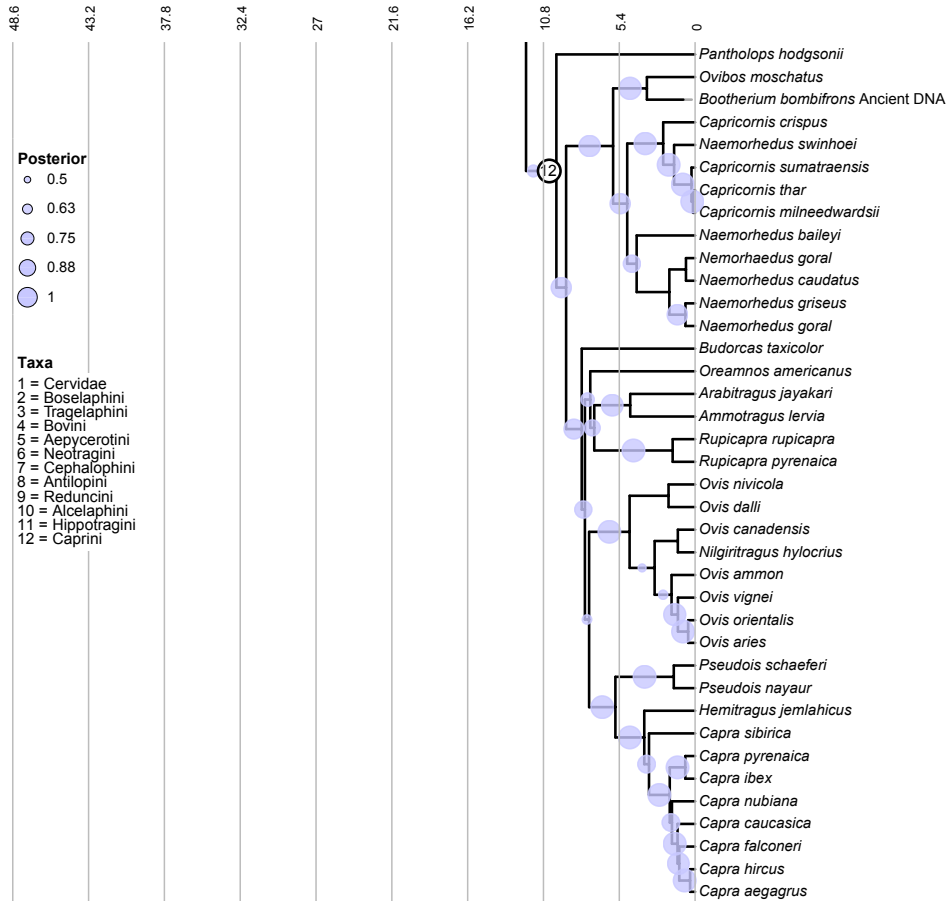


FIGURE 6. Maximum clade credibility Bayesian total evidence topology (opposite page, above, and next page). Extinct species are labeled Ancient DNA or Fossil to denote how they appear in the matrix. Posterior probabilities for each node over 0.5 are represented as scaled circles. Divergence dates estimated from fossil calibrations are represented in millions of years. Note the estimated divergence time of the clade Oreotragini + Cephalophini + Antilopini was older than the estimated divergence of the rest of Antilopinae in which it belongs.



and Moen, 2008; Wiens and Morrill, 2011). Within total evidence analyses, missing morphological data can influence recovery of the “correct” topology (Sansom and Wills, 2013, 2017; Pattinson et al., 2015; Guillaume and Cooper, 2016); however, the inclusion of morphological data for at least half the living species in the total evidence matrix can remedy this issue (Guillaume and Cooper, 2016). The total evidence matrix here includes morphological data for 75 extant species (52% of all living species included in the matrix). Different types of morphological characters (i.e., dental, osteological, soft tissue) display varying levels of homoplasy within mammals, and thus may provide conflicting evidence of phylogenetic relationships when some types of data are missing for fossil species (Sansom and Wills, 2013, 2017; Sansom et al., 2017). Coding more morphological characters for more extant taxa could help alleviate this issue, especially by filling in gaps where the characters available for fossil species may not have been coded for living species to which they are related. The extant species correctly placed on the basis of morphological characters alone suggests that the failure of some fossil species to align in this study with their most likely tribes may be attributed to the lack of close relatives and evolutionary distance between them and extant representatives of their tribes.

## SYNAPOMORPHIES

The ultimate goal of this study was to find hard-tissue synapomorphies for the family Bovidae by optimizing morphological characters on a total evidence phylogeny, testing whether a total evidence phylogeny could provide synapomorphies for the clades that are of use in determining fossil relationships to Bovidae. Historically, the defining synapomorphy for Bovidae has been the presence of permanent, unbranched horn cores covered by permanent, unbranched keratin sheaths (Gray, 1821; Pilgrim, 1946; Janis and Scott, 1987; Bibi et al., 2009). The lack of preservation of horn sheaths in the fossil record, the great amount of homoplasy in the family, and the variable presence of horns in females have made it difficult not only to place fossil species in the family, but also to expand the list of diagnostic characters beyond the presence of permanent, unbranched horn cores (Bibi et al., 2009). An analysis by Pilgrim (1946) aligned *Eotragus* with Bovidae based on the presence of horn cores, selenodont molars with four distinct crescents, upper premolars with a single enamel crescent, and complex enamel folds on the lower premolars, which he proposed distinguish Bovidae from Gelocidae (Pilgrim, 1946).

Janis and Scott (1987) found several derived characters for Bovidae in their analysis, but rejected them as synapomorphies because of homoplasy with other ruminant families. These characters included hypsodont molars and elongated limbs without lateral digits, which are common among other nonbovid ruminants in open habitats; “fused metatarsals with an open gully,” shared with members of Giraffoidea; and entostyles on upper molars, which bovids share with brachydont members of Cervoidea (Janis and Scott, 1987). Although the shape and position of the auditory bulla may be diagnostic for some bovids, they noted that many species do not have an expanded bulla at all; based on their interpretation of these characters and the scope of their morphological data, they determined that the presence of horns was the only diagnostic character of Bovidae (Janis and Scott, 1987).

Gentry’s (1992) analysis of morphological characters produced several synapomorphies for tribes and other subclades of Bovidae, but the topology proposed by his analysis diverges strongly from the topology produced by molecular data; as a result, comparing his tribal level synapomorphies to the results of this study presents several challenges. On his topology, the clade most resembling Bovidae for which he reports synapomorphies excludes *S. grimmia*, *T. scriptus*, and *T. quadricornis*. Seven of his characters map as synapomorphies for this clade: an inclined cranial roof, a braincase with parallel sides or sides that widen anteriorly, large postglenoid foramen, foramina ovalia opening laterally, lack of basal pillars on all upper and some lower molars, a large indent on the femur between the articular head and the greater trochanter, and distal flanges on the radius (Gentry, 1992).

My analysis produced two sets of characters that map as bovid synapomorphies: one set based on the full topology, and one on the topology with incorrectly placed fossil taxa removed. I found the full-topology synapomorphies, although fewer than those from the reduced topology, conformed better to the character states found in the data matrix. These characters were useful for aligning only two of the fossil species, *G. lydekkeri* and *T. grangeri*, with Bovidae because they were not scored for the other fossil taxa in this matrix;

however, their broad distribution among the extant species of Bovidae supports their value for future studies.

Two of the synapomorphies identified here share some similarities with the hypsodont molar and anteriorly positioned tympanic bulla that Janis and Scott (1987) proposed as potential diagnostic traits for Bovidae. The mesodont molar synapomorphy of my analysis may simply be a different way of defining and coding one of these characters; their paper distinguishes between only brachyodont and hypsodont crown heights, defining any tooth with crown height greater than the tooth width as hypsodont (Janis and Scott, 1987), whereas in the data analyzed here, mesodonta is judged by a range of hypsodonty index values from 1.5 to 3 (Bärmann, 2013, 2014). Their broader definition of hypsodonty thus encompasses the mesodonty of this paper, and potentially obscures a character that could serve as a synapomorphy. Hypsodonty is rightly recognized a highly plesiomorphic character, thus using this synapomorphy for distinguishing between bovids and other ruminants requires great care (Janis and Scott, 1987; Janis and Theodor, 2014). I recommend considering hypsodonty only in combination with other synapomorphies for the family. The auditory bulla character state that mapped as a synapomorphy in this analysis also differentiated between more levels of inflation than Janis and Scott (1987). Although it is consistent across many of the species in this matrix, the character is not coded for several tribes, and so should be treated as a tentative synapomorphy from this analysis.

Synapomorphies from this study could link fossil species with Aepycerotini, Antilopini, Bovini, Caprini, and Reduncini, out of the nine tribes with fossil representatives. Long, uncompressed, lyre-shaped horn cores and a large, deep postcornual fossa were among the characteristics that diagnose *Aepyceros*, the only genus in Aepycerotini (Gentry, 2011). These characters both mapped as synapomorphies for the tribe and supported including *A. shungurae* in the clade. A transverse metaconid ridge on p3 (char. 55, state 1), which mapped as a synapomorphy in this study, could expand the list of features that define Aepycerotini. Gentry (1992) found few monophyletic tribes that agree with large-scale molecular or combined-evidence analyses, but his analysis did reconstruct monophyletic Antilopini. One character, fusion of the metaconid and entoconid of p4, was a synapomorphy on both his morphological phylogeny and my total evidence phylogeny, which could link *G. lydekkeri* to Antilopini. This character was not exclusive to Antilopini on this phylogeny, thus it requires corroboration from other characters when assessing fossil relationships. Geraads (1992) proposed an inclined horn core synapomorphy for Bovini. Although the character differs in describing the inclination in my analysis, it linked *U. gautieri* to Bovini. This synapomorphy, along with a suite of other horn core characters, also supports the inclusion of the genus *Brabovus*, not analyzed here, in Bovini (Geraads, 1992). Short metacarpals are a traditional character defining Caprini (Bibi et al., 2012). The analysis in this study found several new craniodental synapomorphies that could be used for fossil placements, and could especially benefit attempts to reassess the large number of fossil caprines potentially incorrectly referred to the family (Gentry, 2000). Previous research identifies at least four cranial and dental characters that support Reduncini: the high anterior angle of the horn cores, the low angle of the face relative to the braincase in lateral view, prominent

“goat fold” anterior cingulids (*sensu* Bärmann and Rössner, 2011) on the molars, and prominent ectostyles/-stylids (Vrba et al., 1994). The character identified in this study that could link *K. subdolos* and *S. palaeindicus* to Reduncini, a braincase the same width along the anteroposterior axis, thus represents a new potential synapomorphy for the clade.

Although character optimizations here produced synapomorphies throughout Bovidae, they must be tested against other fossil species in future analyses. For example, it is unclear whether some species of *Eotragus*, among other purported early bovids, are stem or crown bovids (Solounias et al., 1995; Bibi, 2007; Bibi et al., 2009), and assignment of some fossil species to certain tribes are contradicted by different analyses. There are many fossil taxa that could benefit from inclusion in a large-scale analysis with a goal toward refining their position in Bovidae, such as *Brabovus nanincisus*, which could belong in Bovini, Tragelaphini, or Cephalophini (Gentry, 2011). Likewise, using these characters in efforts to revise the positions of taxa currently considered stem species of Moschidae or other ruminant families could test the value of these characters as bovid synapomorphies. Recent studies of these fossils provide rich sets of morphological characters, unfortunately few of which overlap with the morphological synapomorphies in this study. The presence of P2 and P3 of equivalent size (char. 119, state 2) may be found in *Propalaeoryx*, considered part of the Giraffoid family Climacoceratidae, and *Namacerus*, a likely stem bovid (Morales et al., 2003). Presence of a single lacrimal foramen (char. 154, state 1) is shared by several fossil species (e.g., *Dremotherium*, *Amphimoschus*, *Ampelomeryx*) from across the ruminant tree, but not cervids and antilocaprids (Mennecart et al., 2021). In a future analysis of these characters in the broader context of ruminants, this character may not optimize as a synapomorphy of Bovidae, but could instead serve as morphological support for the relationship between Bovidae and Moschidae. Two synapomorphies for Bovidae, inflation of the tympanic bulla to the level of the occipital condyle (char. 176, state 1) and mesodont molars (char. 138, state 1), are similar to descriptions of fossils in recent studies, but require clarification before they could be used to support inferences of relationships. *Spergebietomeryx*, likely part of the Climacoceratidae, may have an inflated tympanic bulla (Morales et al., 2008). *Namacerus* is described as having “slightly hypsodont” molars (Morales et al., 2003), and *Namibiomeryx* exhibits “incipient hypsodonty” (Morales et al., 2008). Reexamining these species with quantitative versions of these characters (e.g., defining hypsodonty based on a range of hypsodonty index values) could better elucidate the anatomy’s variation, evolution, and value as a diagnostic synapomorphy. By examining these species for synapomorphies identified in this study and expanding the dataset to include these species in further phylogenetic analyses, we could achieve a more complete picture of bovid, and even ruminant, evolutionary history.

## CONCLUSIONS

Total evidence phylogenetic analyses provide a promising method for unraveling the complex history of Bovidae. In this analysis, new synapomorphic characters were discovered that support

the placement of fossils within Bovidae and several tribes. Although the morphological characters in these data did not place many of the fossils in the expected tribes during the phylogenetic analysis, multiple synapomorphies were robust to the presence of these species in the phylogeny. Approaches that algorithmically apply weights to morphological characters, such as TNT's implied weighting (Goloboff, 2014) or RAxML's evolutionary placement algorithm (Berger and Stamatakis, 2011), may provide more reliable estimates of the fossil relationships, potentially revealing a different set of synapomorphic characters. Only cranial characters mapped as synapomorphies for Bovidae in this analysis, precluding their use with fossil taxa known only from incomplete crania or postcranial material. Future studies must increase the number of morphological characters, the types of morphological features surveyed, and the number of fossil and living species for which morphological characters are encoded to take full advantage of the rich fossil record in addressing questions of bovid relationships, potentially providing better support for relationships here or overturning poorly supported molecular relationships.

#### ACKNOWLEDGMENTS

The author thanks J. Flynn, N. Simmons, D. Barta, M. Tessler, and two anonymous reviewers for feedback on research design and comments that improved the manuscript. This research was possible through fellowship support from the Richard Gilder Graduate School and NSF IGERT training grant (DGE-0966166) awarded through the Richard Gilder Graduate School.

#### REFERENCES

- Barbera, P., et al. 2019. EPA-ng: Massively parallel evolutionary placement of genetic sequences. *Systematic Biology* 68: 365–369.
- Barido-Sottani, J., et al. 2018. Taming the BEAST—a community teaching material resource for BEAST 2. *Systematic Biology* 67: 170–174.
- Bärmann, E.V. 2013. Towards a comprehensive phylogeny of Bovidae (Ruminantia, Artiodactyla, Mammalia). Ph.D. dissertation, Zoology, University of Cambridge, 242 pp.
- Bärmann, E.V. 2014. The evolution of body size, horn shape and social behaviour in crown Antilopini – an ancestral character state analysis. *Zitteliana B* 32: 185–196.
- Bärmann, E.V., and G.E. Rössner. 2011. Dental nomenclature in Ruminantia: towards a standard terminological framework. *Mammalian Biology* 76: 762–768.
- Bärmann, E.V., and T. Schikora. 2014. The polyphyly of *Neotragus* – results from genetic and morphometric analyses. *Mammalian Biology* 79: 283–286.
- Bärmann, E.V., G.E. Rössner, and G. Wörheide. 2013. A revised phylogeny of Antilopini (Bovidae, Artiodactyla) using combined mitochondrial and nuclear genes. *Molecular Phylogenetics and Evolution* 67: 484–93.
- Berger, S.A., and A. Stamatakis. 2011. Aligning short reads to reference alignments and trees. *Bioinformatics* 27: 2068–2075.
- Berger, S.A., D. Krompass, and A. Stamatakis. 2011. Performance, accuracy, and web server for evolutionary placement of short sequence reads under maximum likelihood. *Systematic Biology* 60: 291–302.

- Bibi, F. 2007. Origin, paleoecology, and paleobiogeography of early Bovini. *Palaeogeography, Palaeoclimatology, Palaeoecology* 248: 60–72.
- Bibi, F. 2013. A multi-calibrated mitochondrial phylogeny of extant Bovidae (Artiodactyla, Ruminantia) and the importance of the fossil record to systematics. *BMC Evolutionary Biology* 13: 166.
- Bibi, F. 2014. Assembling the ruminant tree: combining morphology, molecules, extant taxa, and fossils. *Zitteliana B* 32: 197–212.
- Bibi, F., et al. 2009. The fossil record and evolution of Bovidae: state of the field. *Palaeontologia Electronica* 12.
- Bibi, F., E. Vrba, and F. Fack. 2012. A new African fossil caprin and a combined molecular and morphological Bayesian phylogenetic analysis of Caprini (Mammalia: Bovidae). *Journal of Evolutionary Biology* 25: 1843–1854.
- Bouckaert, R.R., and A.J. Drummond. 2017. bModelTest: Bayesian phylogenetic site model averaging and model comparison. *BMC Evolutionary Biology* 17.
- Calamari, Z.T. 2016. Sexual maturity and shape development in cranial appendages of extant ruminants. *Ecology and Evolution* 6 (21): 7820–7830.
- Cantalapiedra, J.L., G.M. Alcalde, and M. Hernández Fernández. 2014. The contribution of phylogenetics to the study of ruminant evolutionary ecology. *Zitteliana B* 32: 47–52.
- Cantalapiedra, J.L., M. Hernández Fernández, B. Azanza, and J. Morales. 2015. Congruent phylogenetic and fossil signatures of mammalian diversification dynamics driven by Tertiary abiotic change. *Evolution* 69: 2941–2953.
- Chen, L., et al. 2019. Large-scale ruminant genome sequencing provides insights into their evolution and distinct traits. *Science* 364.
- Cohen, K.M., S.C. Finney, P.L. Gibbard, and J.-X. Fan. 2013. The ICS International Chronostratigraphic Chart. *Episodes* 36: 199–204.
- Dávalos, L.M., P.M. Velazco, O.M. Warsi, P.D. Smits, and N.B. Simmons. 2014. Integrating incomplete fossils by isolating conflicting signal in saturated and non-independent morphological characters. *Systematic Biology* 63: 582–600.
- Decker, J.E., et al. 2009. Resolving the evolution of extant and extinct ruminants with high-throughput phylogenomics. *Proceedings of the National Academy of Sciences of the United States of America* 106: 18644–18649.
- Delsuc, F., et al. 2016. The phylogenetic affinities of the extinct glyptodonts. *Current Biology* 26: R155–R156.
- DeMiguel, D., B. Azanza, and J. Morales. 2014. Key innovations in ruminant evolution: a paleontological perspective. *Integrative Zoology* 9: 412–433.
- Eernisse, D.J., and A.G. Kluge. 1993. Taxonomic congruence versus total evidence, and amniote phylogeny inferred from fossils, molecules, and morphology. *Molecular Biology and Evolution* 10: 1170–1195.
- Engel, J. 2004. Morphology and genetics. In T. Gilbert and T. Woodfine (editors), *The biology, husbandry and conservation of scimitar-horned oryx (Oryx dammah)*, 2nd ed.: 3. Marwell Preservation Trust.
- Fernández, M.H., and E.S. Vrba. 2005. A complete estimate of the phylogenetic relationships in Ruminantia: a dated species-level supertree of the extant ruminants. *Biological Reviews* 80: 269–302.
- Gatesy, J., and P. Arctander. 2000. Hidden morphological support for the phylogenetic placement of *Pseudoryx nghetinhensis* with bovine bovids: a combined analysis of gross anatomical evidence and DNA sequences from five genes. *Systematic Biology* 49: 515–538.

- Gatesy, J., D. Yelon, R. DeSalle, and E.S. Vrba. 1992. Phylogeny of Bovidae (Artiodactyla, mammalia), based on mitochondrial ribosomal DNA sequences. *Molecular Biology and Evolution* 9: 433–446.
- Gentry, A.W. 1992. The subfamilies and tribes of the family Bovidae. *Mammal Review* 22: 1–32.
- Gentry, A.W. 2000. Caprinae and Hippotragini (Bovidae, Mammalia) in the Upper Miocene. *In* E.S. Vrba and G.B. Schaller (editors), *Antelopes, deer, and relatives: fossil record, behavioral ecology, systematics, and conservation*: 65–83. New Haven, CT: Yale University Press.
- Gentry, A.W. 2011. Bovidae. *In* T. Harrison (editor), *Paleontology and geology of Laetoli: human evolution in context*. Vol. 2, Fossil hominins and the associated fauna: 363–465. Dordrecht: Springer Netherlands.
- Geraads, D. 1992. Phylogenetic analysis of the tribe Bovini (Mammalia: Artiodactyla). *Zoological Journal of the Linnean Society* 104: 193–207.
- Geraads, D. 2003. Ruminants, other than Giraffidae from the middle Miocene hominoid locality of Çandır (Turkey). *Courier Forschungsinstitut Senckenberg* 240: 181–199.
- Gilbert, T. 2017. *International studbook for the scimitar-horned oryx Oryx Dammah*, 12th ed. Winchester, United Kingdom: Marwell Wildlife.
- Goloboff, P.A. 2014. Extended implied weighting. *Cladistics* 30: 260–272.
- Gray, J.E. 1821. On the natural arrangement of vertebrate animals. *London Medical Repository* 15: 296–310.
- Guillermé, T., and N. Cooper. 2016. Effects of missing data on topological inference using a total evidence approach. *Molecular Phylogenetics and Evolution* 94: 146–158.
- Hagelberg, E., M. Hofreiter, and C. Keyser. 2015. Ancient DNA: the first three decades. *Philosophical Transactions of the Royal Society B, Biological Sciences* 370: 20130371.
- Hassanin, A., E. Pasquet, and J.-D. Vigne. 1998. Molecular systematics of the subfamily Caprinae (Artiodactyla, Bovidae) as determined from cytochrome *b* sequences. *Journal of Mammalian Evolution* 5: 217–236.
- Hassanin, A., et al. 2012. Pattern and timing of diversification of Cetartiodactyla (Mammalia, Laurasiatheria), as revealed by a comprehensive analysis of mitochondrial genomes. *Comptes Rendus Biologies* 335: 32–50.
- Hassanin, A., J. An, A. Ropiquet, T.T. Nguyen, and A. Couloux. 2013. Combining multiple autosomal introns for studying shallow phylogeny and taxonomy of Laurasiatherian mammals: application to the tribe Bovini (Cetartiodactyla, Bovidae). *Molecular Phylogenetics and Evolution* 66: 766–775.
- Heath, T.A., J.P. Huelsenbeck, and T. Stadler. 2014. The fossilized birth-death process for coherent calibration of divergence-time estimates. *Proceedings of the National Academy of Sciences of the United States of America* 111: E2957–E2966.
- Hedtke, S.M., T.M. Townsend, and D.M. Hillis. 2006. Resolution of phylogenetic conflict in large data sets by increased taxon sampling. *Systematic Biology* 55: 522–529.
- Hillis, D.M. 1996. Inferring complex phylogenies. *Nature* 383: 130–131.
- Janis, C.M., and K.M. Scott. 1987. The interrelationships of higher ruminant families with a special emphasis on the members of the Cervoidea. *American Museum Novitates* 2893: 1–85.
- Janis, C.M., and J.M. Theodor. 2014. Cranial and postcranial morphological data in ruminant phylogenetics. *Zitteliana B* 32.
- Johnston, A.R., and N.M. Anthony. 2012. A multi-locus species phylogeny of African forest duikers in the subfamily Cephalophinae: evidence for a recent radiation in the Pleistocene. *BMC Evolutionary Biology* 12: 120.

- Katoh, K., K. Misawa, K. Kuma, and T. Miyata. 2002. MAFFT: a novel method for rapid multiple sequence alignment based on fast Fourier transform. *Nucleic Acids Research* 30: 3059–3066.
- Kozlov, A.M., D. Darriba, T. Flouri, B. Morel, and A. Stamatakis. 2019. RAXML-NG: a fast, scalable and user-friendly tool for maximum likelihood phylogenetic inference. *Bioinformatics* 35: 4453–4455.
- Lanfear, R., P.B. Frandsen, A.M. Wright, T. Senfeld, and B. Calcott. 2017. PartitionFinder 2: new methods for selecting partitioned models of evolution for molecular and morphological phylogenetic analyses. *Molecular Biology and Evolution* 34: 772–773.
- Lewis, P.O. 2001. A likelihood approach to estimating phylogeny from discrete morphological character data. *Systematic Biology* 50: 913–925.
- Marcot, J.D. 2004. Evolutionary radiations of Ruminantia (Mammalia: Artiodactyla). Ph.D. dissertation, Evolutionary Biology, The University of Chicago, 291 pp.
- Marcot, J.D. 2007. Molecular phylogeny of terrestrial artiodactyls: conflicts and resolution. In D.R. Prothero and S.E. Foss (editors), *The evolution of artiodactyls: 4–18*. Baltimore: Johns Hopkins University Press.
- Mennecart, B., G. Métais, L. Costeur, L. Ginsburg, and G.E. Rössner. 2021. Reassessment of the enigmatic ruminant Miocene genus *Amphimoschus* Bourgeois, 1873 (Mammalia, Artiodactyla, Pecora). *PLOS ONE* 16: e0244661.
- Morales, J., D. Soria, M. Pickford, and M. Nieto. 2003. A new genus and species of Bovidae (Artiodactyla, Mammalia) from the early Middle Miocene of Arrisdrift, Namibia, and the origins of the family Bovidae. *Memoir of the Geological Survey of Namibia* 19: 371–384.
- Morales, J., D. Soria, and M. Pickford. 2008. Pecoran ruminants from the early Miocene of the Sperrgebiet, Namibia. *Memoir of the Geological Survey of Namibia* 20: 397–464.
- Pattinson, D.J., R.S. Thompson, A.K. Piotrowski, and R.J. Asher. 2015. Phylogeny, paleontology, and primates: do incomplete fossils bias the tree of life? *Systematic Biology* 64: 169–186.
- Pilgrim, G.E. 1946. The evolution of the buffaloes, oxen, sheep and goats. *Journal of the Linnean Society of London, Zoology* 41: 272–286.
- Queiroz, A. de, and J. Gatesy. 2007. The supermatrix approach to systematics. *Trends in Ecology and Evolution* 22: 34–41.
- Queiroz, A. de, M.J. Donoghue, and J. Kim. 1995. Separate versus combined analysis of phylogenetic evidence. *Annual Review of Ecology and Systematics* 26: 657–681.
- Robinson, T.J., et al. 2014. Phylogeny and vicariant speciation of the grey rhebok, *Pelea capreolus*. *Heredity* 112: 325–332.
- Ropiquet, A. 2017. Two new genera of Bovidae (Mammalia). *Dumerilia* 7: 78–81.
- Ropiquet, A., and A. Hassanin. 2005. Molecular evidence for the polyphyly of the genus *Hemitragus* (Mammalia, Bovidae). *Molecular Phylogenetics and Evolution* 36: 154–168.
- Sansom, R.S., and M.A. Wills. 2013. Fossilization causes organisms to appear erroneously primitive by distorting evolutionary trees. *Scientific Reports* 3: 2545.
- Sansom, R.S., and M.A. Wills. 2017. Differences between hard and soft phylogenetic data. *Proceedings of the Royal Society B: Biological Sciences* 284: 20172150.
- Sansom, R.S., M.A. Wills, and T. Williams. 2017. Dental data perform relatively poorly in reconstructing mammal phylogenies: morphological partitions evaluated with molecular benchmarks. *Systematic Biology* 66: 813–822.
- Solounias, N., J.C. Barry, R.L. Bernor, E.H. Lindsay, and S.M. Raza. 1995. The oldest bovid from the Siwaliks, Pakistan. *Journal of Vertebrate Paleontology* 15: 806–814.
- Stamatakis, A. 2014. RAXML version 8: a tool for phylogenetic analysis and post-analysis of large phylogenies. *Bioinformatics* 30: 1312–1313.

- Stamatakis, A. 2016. The RAxML v8.2.X manual. Online resource (available at <https://cme.h-its.org/exelixis/resource/download/NewManual.pdf>).
- Streicher, J.W., J.A. Schulte II, and J.J. Wiens. 2016. How should genes and taxa be sampled for phylogenomic analyses with missing data? An empirical study in iguanian lizards. *Systematic Biology* 65: 128–145.
- Thomas, H. 1994. Anatomie crânienne et relations phylogénétiques du nouveau bovidé (*Pseudoryx nghetinhensis*) découvert dans la cordillère annamitique au Vietnam. *Mammalia* 58: 453–482.
- Troy, C.S., et al. 2001. Genetic evidence for Near-Eastern origins of European cattle. *Nature* 410: 1088–1091.
- Verkaar, E.L.C., I.J. Nijman, M. Beeke, E. Hanekamp, and J.A. Lenstra. 2004. Maternal and paternal lineages in cross-breeding bovine species. Has wisent a hybrid origin? *Molecular Biology and Evolution* 21: 1165–1170.
- Vrba, E.S. 2006. A possible ancestor of the living waterbuck and lechwes: *Kobus basilcookei* sp. nov. (Reduncini, Bovidae, Artiodactyla) from the Early Pliocene of the Middle Awash, Ethiopia. *Transactions of the Royal Society of South Africa* 61: 63–74.
- Vrba, E.S. and Y. Haile-Selassie. 2006. A new antelope, *Zephyreduncinus oundagaisus* (Reduncini, Artiodactyla, Bovidae), from the Late Miocene of the Middle Awash, Afar Rift, Ethiopia. *Journal of Vertebrate Paleontology* 26: 213–218.
- Vrba, E.S., J.R. Vaisnys, J.E. Gatesy, R. DeSalle, and K.-Y. Wei. 1994. Analysis of paedomorphosis using allometric characters: the example of Reduncini antelopes (Bovidae, Mammalia). *Systematic Biology* 43: 92–116.
- West, A.R. 2016. Mitogenome of the extinct helmeted musk ox, *Bootherium bombifrons*. *Mitochondrial DNA Part B* 1: 862–863.
- Wiens, J.J. 2003. Missing data, incomplete taxa, and phylogenetic accuracy. *Systematic Biology* 52: 528–538.
- Wiens, J.J., and D.S. Moen. 2008. Missing data and the accuracy of Bayesian phylogenetics. *Journal of Systematics and Evolution* 46: 307–314.
- Wiens, J.J., and M.C. Morrill. 2011. Missing data in phylogenetic analysis: reconciling results from simulations and empirical data. *Systematic Biology* 60: 719–731.
- Wu, D.-D., et al. 2018. Pervasive introgression facilitated domestication and adaptation in the *Bos* species complex. *Nature Ecology & Evolution* 2: 1139–1145.
- Xiaoming, W., Z. Qiu, and N.D. Opdyke. 2003. Litho-, bio-, and magnetostratigraphy and paleoenvironment of Tunggur Formation (Middle Miocene) in Central Inner Mongolia, China. *American Museum Novitates* 3411: 1–31.
- Zwickl, D.J., and D.M. Hillis. 2002. Increased taxon sampling greatly reduces phylogenetic error. *Systematic Biology* 51: 588–598.

## APPENDIX 1

## LIST OF MORPHOLOGICAL CHARACTERS AND SOURCES

List includes the character number in the original publication. Sources are G = Gentry, 1992; T = Thomas, 1994; B = Bärmann, 2013, 2014. The number of each character in its original matrix is noted after the citation. Characters that different authors coded differently for the same species were coded as polymorphic in this matrix. Character descriptions are compiled here from their original publications, with minor adjustments for consistent formatting, unless otherwise noted.

1. Horn cores: 0, short; 1, medium; 2, long (G1, T3).
2. Horn cores: 0, without keels; 1, with keels (G4, T6).
3. Horn-core diameter: 0, small; 1, intermediate; 2, larger (G5, T7).
4. Horn cores: 0, without transverse ridges; 1, with transverse ridges (G6, T8).
5. Horn cores inserted: 0, above orbits; 1, behind orbits (G7, T9).
6. Horn cores: 0, a little inclined in side view; 1, much inclined in side view (G8, T10).
7. Horn cores: 0, a little inclined; 1, upright (G9, T11).
8. Horn cores inserted: 0, widely apart; 1, intermediate; 2, closer (G10, T12).
9. Horn cores: 0, without grooves. 1, with moderate grooves; 2, with deep longitudinal grooves (G11, T13).
10. Horn cores: 0, a little divergent; 1, very divergent (G12, T14).
11. Females: 0, without horns; 1, with horns (G15, T17, B77; Gentry and Thomas states recoded based on horn length data from Calamari (2016) and sources within. Coded as polymorphic for states 1 and 2 if no data available).
12. Postcornual fossa: 0, absent; 1, poor or definite (G16, T18, B74).
13. Dorsal orbital rims: 0, narrow; 1, wide (G17, T19).
14. Frontals: 0, without internal sinuses; 1, with moderate internal sinuses; 2, with extensive internal sinuses (G18, T20).
15. Cranial roof: 0, slightly inclined; 1, much angled or curved down posteriorly (G19, T21).
16. Cranial roof: 0, slightly inclined; 1, horizontal (G20, T22).
17. Interfrontal suture: 0, simple; 1, moderate; 2, complicated or raised as a ridge (G21, T23).
18. Supraorbital foramina: 0, without surrounding pits; 1, with surrounding pits (G22, T24).
19. Braincase sides widening: 0, posteriorly; 1, parallel; 2, anteriorly (G23, T25).
20. Supraorbital foramina placed forwards and widely apart (G24, T26).
21. Temporal ridges: 0, approach closely posteriorly; 1, approach moderately; 2, are wide apart (G25, T27).
22. Zygomatic arch: 0, not deepened under orbit; 1, moderately deepened under orbit; 2, much deepened under orbit (G26, T28).
23. Face lengthened (G27, T29).
24. Back of adult tooth row: 0, behind level of front of orbit; 1, below or anterior to level of front of orbit (G28, T30).

25. Lacrimal: 0, small; 1, moderate; 2, expanded (G29, T31).
26. Jugal: 0, small; 1, expanded (G30, T32).
27. Jugal: 0, without clear lobes; 1, with two lobes (G31, T33).
28. Maxillary tuberosity: 0, insignificant; 1, moderate; 2, prominent (G32, T34).
29. Ethmoidal fissure absent (G33, T35).
30. Preorbital fossa absent (G34, T36).
31. Infraorbital foramen: 0, low and anterior; 1, high and more posterior (G35, T37).
32. Lateral flanges at front of nasals: 0, present; 1, absent (G36, T38).
33. Premaxilla: 0, contacting nasals; 1, not contacting nasals (G37, T39, B30; character states from Bärmann were reversed, i.e., state 0 recoded as 1, state 1 recoded as 0, to match Gentry/Thomas).
34. Palatal ridges in front of tooth rows: 0, approach each other; 1, approach and touch (G38, T40).
35. Vomer fusion with palate passes far posteriorly (G39, T41).
36. Palatine foramina: 0, of normal width apart; 1, nearer teeth (G40, T42).
37. Palatine foramina: 0, of normal width apart; 1, nearer midline of palate (G41, T43).
38. Palatine foramina situated posteriorly (G42, T44, B51).
39. Median indent at back of palate: 0, posterior to lateral indents; 1, slightly anterior to lateral indents; 2, very anterior to lateral ones (G43, T45).
40. Auditory bulla: 0, small; 1, larger (G44, T46).
41. Basioccipital: 0, triangular; 1, rectangular; 2, very wide anteriorly (G45, T47).
42. Anterior tuberosities of basioccipital: 0, weak; 1, strong or localized (G46, T48).
43. Anterior tuberosities with strong longitudinal ridges behind them (G47, T49).
44. Postglenoid foramina: 0, absent or small; 1, present, perhaps larger (G48, T50).
45. Foramina ovalia: 0, smaller; 1, intermediate; 2, large (G49, T51, B62; character state 1 in Bärmann recoded as state 2 to match Gentry/Thomas).
46. Foramina ovalia open more: 0, ventrally; 1, laterally (G50, T52).
47. Occipital surface: 0, faces partly laterally on each side; 1, faces posteriorly (G51, T53).
48. Mastoid exposure: 0, wide; 1, narrow (G52, T54).
49. Mastoid exposure: 0, posterior; 1, lateral (G53, T55).
50. Mastoid contacts parietal (G54, T56).
51. First incisors: 0, small; 1, moderate; 2, enlarged (G55, T57).
52. Cheek teeth: 0, low crowned; 1, high crowned (G56, T58).
53. Length of premolar row less than 60% molar row length (G57, T59).
54. p2: 0, always present; 1, sometimes absent (G58, T60, B13).
55. p3 metaconid ridge: 0, oblique; 1, transverse (G59, T61).
56. Paraconid of p3 and p4: 0, indistinct; 1, well separated from parastyloid (G60, T62, B14; character states from Bärmann reversed to match Gentry/Thomas).
57. p4 with labial origin of metaconid situated posterior to protoconid (G61, T63).
58. p4 with: 0, shallow labial valley; 1, deep labial valley anterior to hypoconid (G62, T64).
59. Metaconid-entoconid: 0, not fused; 1, fused lingually on p4 (G63, T65).

60. Paraconid and metaconid fused on p4 (G64, T66).
61. Upper molar entostyles: 0, small; 1, absent (G65, T67).
62. Upper molar entostyles: 0, small; 1, enlarged (G66, T68).
63. Upper molar mesostyles strong and with concave labial wall of metacone behind (G67, T69).
64. M3 metastyle as a flange: 0, weak; 1, moderate; 2, strong (G68, T70).
65. Upper molars with large or localized labial ribs between the styles (G69, T71).
66. Upper molars with: 0, simple; 1, complicated outline of central cavities (G70, T72).
67. Upper molars with small additional cavities near central lingual edge of occlusal surface (G71, T73).
68. Back half of M3 enlarged (G72, T74).
69. Ectostylids: 0, on all lower molars; 1, lost in m2–m3; 2, lost in m1–m3 (G73, T75, B19).
70. Lower molars with: 0, outbowed; 1, flat lingual walls (G74, T76).
71. lower molars: 0, with transverse anterior cingulid “goat folds”; 1, without transverse anterior cingulids (G75, T77).
72. m3 hypoconulid offset labialwards (G76, T78).
73. m3 hypoconulid: 0, without; 1, with a central cavity until middle or later wear (G77, T79).
74. Metacarpal much lengthened (G78, T80).
75. Radius long than metacarpal and much longer than humerus (G79, T81).
76. Metacarpal notably shortened (G80, T82).
77. Femur with: 0, weak; 1, strong indent between articular head and greater trochanter (G81, T83).
78. Vastus lateralis crest passing above and behind crest for gluteus accessorius (G82, T84).
79. Top of greater trochanter: 0, narrow; 1, wide relative to its own narrower lower part in lateral view (G83, T85).
80. Lateral part of articular head: 0, narrow; 1, wide in dorsal view (G84, T86).
81. Lateral roughened fossa distally on posterior surface of shaft is deep and/or extends higher on shaft (G85, T87).
82. Patellar fossa: 0, normal width; 1, wide (G86, T88).
83. Protuberance above distal lateral condyle: 0, weak; 1, strong in posterior view (G87, T89).
84. Tibia with strong tubercle and well-marked adjacent medial hollow at center front of top articular surface (G88, T90).
85. Lateral edge of latera facet upcurved (G89, T91).
86. Patellar groove: 0, absent; 1, present on front top of cnemial crest (G90, T92).
87. Longitudinal digital flexor ridge on posterior surface lying: 0, medially; 1, more laterally (G91, T93).
88. Metatarsal has main naviculocuboid facet: 0, large; 1, smaller (G92, T94).
89. Posteromedial part of main naviculocuboid facet is raised in medial view (G93, T95).
90. Hollow at top of posterior surface: 0, stronger; 1, insignificant (G94, T96).
91. Mediolateral compression of shaft: 0, normal; 1, reduced (G95, T97).

92. Longitudinal groove on anterior surface: 0, stronger; 1, weak (G96, T98).
93. Flanges distally on anterior surface: 0, strong; 1, weak (G97, T99).
94. Humerus lateral tuberosity: 0, rising; 1, not rising above infraspinatus insertion in lateral view (G98, T100).
95. Lateral tuberosity: 0, upright; 1, curved medially above bicipital groove (G99, T101).
96. Posterior eminence becomes a flange behind infraspinatus (G100, T102).
97. Bicipital groove: 0, narrow; 1, wide (G101, T103).
98. Top of medial tuberosity: 0, pointed; 1, not pointed (G102, T104).
99. Base of medial tuberosity squared off in anterior view (G103, T105).
100. Top of distal medial condyle: 0, cut away; 1, expanded (G104, T106).
101. Radius with medial rim on proximal medial facet (G105, T107).
102. Back of medial facet projects: 0, little; 1, much (G106, T108).
103. Back edge of lateral facet set forwards (G107, T109).
104. Lateral tubercle: 0, small and low; 1, large and high (G108, T110).
105. Distal flanges on anterior side: 0, wide; 1, close (G109, T111).
106. Top of scaphoid facet posteriorly: 0, shallow; 1, deep (G110, T112).
107. Metacarpal: 0, with; 1, without a medial prominence on magnum-trapezoid facet (G111, T113).
108. Top articular surface: 0, indented; 1, not indented posteriorly (G112, T114).
109. Braincase sides widening: 0, posteriorly; 1, more or less parallel (G Fossil Matrix 13).
110. Temporal crests behind horn cores (G Fossil Matrix 14).
111. Basioccipital: 0, triangular; 1, rectangular (G Fossil Matrix 19).
112. Horn cores with flattened lateral surface (G Fossil Matrix 2).
113. Basioccipital with central longitudinal groove or strong anterior tuberosities (G Fossil Matrix 20).
114. Paraconid and metaconid fused or almost fused on p4 (G Fossil Matrix 28).
115. Upper molar mesostyles strong and with flattened or concave labial wall of metacone behind (G Fossil Matrix 31).
116. Sinuses within frontal and horn core pedicle (G Fossil Matrix 7).
117. Upper canines: 0, present; 1, absent (T1).
118. Frontal appendages: 0, absent; 1, present (T2).
119. P2: 0, usually absent; 1, present, reduced (fewer tooth crown elements than P3); 2, present and of similar size as P3 (B1).
120. P2 and P3 length relative to P4: 0, much longer (length of P2 and/or P3 is at least 120% of the length of P4); 1, same length or shorter (B2).
121. Length of upper premolar row relative to length of total upper tooth row: 0, 42% or more; 1, 35%–41%; 2, 34% or less (B3).
122. Upper molar entostyles: 0, absent; 1, always present and relatively big; 2, lambda shaped on at least one of the molars (B4).
123. Upper molar styles: 0, prominent; 1, very small/almost absent (B5).
124. Labial ribs on paracone and metacone of upper molars: 0, absent; 1, present but weak, more prominent on paracone, sometimes only present on M3; 2, present and large on all molars (B6).

125. Thick labial cementum layer on upper molars: 0, absent; 1, present (B7).
126. Central fossetta on upper molars: 0, absent; 1, present (B8).
127. Upper molar lingual cristae (postprotocrista and premetaconulecrista): 0, unfused; at least in young individuals; 1, fused (B9).
128. Size of posterior half of M3 relative to anterior half: 0, same size; 1, distinctly smaller (B10).
129. M3 metastyle: 0, absent or weak; 1, moderate; 2, strong (B11).
130. Lower incisor insertion line: 0, half circle/triangle; 1, only slightly arched (B12).
131. Mesolingual conid (metaconid) of p4: 0, straight; 1, oblique, leaning posteriorly (B15).
132. Anterior conid (paraconid) and mesolingual conid (metaconid) of p4: 0, separate; 1, fused via anterolingual cristid (B16).
133. Mesolingual conid (metaconid) and posterolingual conid (entoconid) of p4: 0, separate; 1, fused via posterolingual cristid (B17).
134. Labial incision on p4: 0, always absent or weak; 1, variable, but deep in some species (B18).
135. Lower molar ectostylid size: 0, absent or low, not connected to postmetacristid and preentocristid until late in life; 1, high, forming part of occlusal plane at least on one molar. (B20).
136. Very pronounced anterior cingulid on lower molars: 0, absent or very weak (tooth slightly elongate, could have a prominent anterior stylid); 1, present on at least m3 (B21).
137. Third lobe of m3: 0, absent; 1, present but very small, consisting of hypoconulid only; 2, present, consisting of hypoconulid only; 3, present, consisting of hypoconulid and entoculid (central fossa visible until middle or later wear) (B22).
138. Cheek tooth height represented as hypsodonty index (HI, height of m3 divided by width of m3): 0, low crowned, brachyodont,  $HI < 1.5$ ; 1, higher crowned, mesodont,  $1.5 < HI < 3$ ; 2, high crowned, hypsodont,  $3 < HI$  (B23).
139. Length of diastema relative to length of cheek tooth row: 0,  $< 50\%$ ; 1,  $50\% - 75\%$ ; 2,  $> 75\%$  (B24).
140. dP3 shape: 0, molariform with anterior part smaller than posterior part (no protocone, but protocrista forming the lingual wall of anterior half); 1, molariform, anterior half and posterior half have the same size (protocone present) (B25).
141. dP2 width compared to dP3: 0, approximately same width; 1, much narrower (B26).
142. dp2 morphology: 0, simple, conical; 1, trenchant tooth with small talonid; 2, with central conid and anterior and posterior accessory cuspids and small talonid with central cusp (protoconulid), total number of cuspids is three to four (B27).
143. Face length (skull anterior to eyes) as % of total condylo-basal length: 0, long,  $46\% - 56\%$ ; 1, elongate,  $57\% - 67\%$ ; 2, very elongate,  $> 67\%$  (B28).
144. Processus nasalis of premaxilla: 0, very short (ends shortly behind foramen incisivum); 1, short, ends in distal half of diastema, not reaching premolars; 2, intermediate length, extending to premolars, sometimes overlapping with P2 or even P3; 3, long, extending to over P3 or even P4; 4, very long, extending to molars (B29).
145. Premaxilla and lacrimal: 0, far apart, never in contact; 1, very close, sometimes in contact; 2, always in contact (B31).
146. Nasal length as % of palatal length: 0, very short, less than  $33\%$ ; 1, short,  $33\% - 42\%$ ; 2, intermediate,  $43\% - 60\%$ ; 3, long,  $61\% - 69\%$ ; 4, very long, more than  $70\%$  (B32).

147. Nasal shape: 0, short, the length is only 100% of the width or less; 1, intermediate, the length is about 150%–250% of the width; 2, long, length is clearly more than 250% of the width; 3, very long and narrow, length is more than 500% of the width (B33).

148. Nasal, middle part with distinct ventrolateral expansion, extending between maxillary and frontal: 0, absent; 1, present (B34).

149. Rostral processes of nasal: 0, median process short, lateral processes clearly present; 1, median process long, lateral processes absent or tiny (B35).

150. Border of nasal and maxillary (and premaxillary, lacrimal): 0, no suture (gap); 1, suture (B36).

151. Nasal and lacrimal: 0, no contact; 1, contact (B37).

152. Preorbital fossa (lacrimal pit): 0, absent; 1, present (at least in males); 2, present and very deep, sharp edge in dorsal part of lacrimal (B38).

153. Facial portion of lacrimal bone relative to orbital diameter: 0, moderate, 65%–90%; 1, large, 91%–130%; 2, very large, more than 131% (B39).

154. Number of lacrimal foramina: 0, two; 1, one (B40).

155. Fenestra in rostrum at junction of lacrimal, nasal, frontal, and maxilla (ethmoidal fissure/antorbital vacuity): 0, absent; 1, present, fissure between nasal and lacrimal (at least in males); 2, enlarged (at least in males) (B41).

156. Fenestra between premaxilla and maxilla: 0, absent; 1, present (B42).

157. Position of infraorbital foramen: 0, in front of toothrow or above P2 (up to P2/P3 boundary, but never clearly above P3); 1, above P2/P3 or P3 (can be variable, but clearly above P3 in some specimens); 2, above P4 or further posterior (B43).

158. Maxilla and frontal: 0, wide apart, never in contact; 1, very close, sometimes in contact (B44).

159. Width across orbits compared to braincase width: 0, narrow, less than 120%; 1, intermediate, 120%–135%; 2, wide, more than 135%–160%; 3, very wide, more than 160% (B45).

160. Small process on squamosal above external auditory meatus: 0, absent; 1, present (B47).

161. Additional suture in squamosal above external auditory meatus, perpendicular to suture between squamosal and parietal: 0, absent; 1, present (B48).

162. Postglenoid foramen (foramen retroarticularis) in dorsal view: 0, visible; 1, not visible (B49).

163. Postglenoid process (processus retroarticularis) at mandibular fossa: 0, absent; 1, present at posteromedial side of mandibular fossa; 2, present and very high and wide (B50).

164. Distance between palatine foramina: 0, encompassing 39% of the palate or less; 1, encompassing 40%–49% of the palate; 2, encompassing 50%–59% of the palate; 3, encompassing more than 60% of the palate (B52).

165. Palatal ridges of maxilla: 0, very close together, sometimes touching each other; 1, further apart, on palatal part of maxillary (B53).

166. Posterior margin of external nares: 0, anterior half of diastema; 1, posterior half of diastema, in front of P2; 2, posterior to P2 (B54).

167. Width of maxilla in front of teeth: 0, slender, equal to width of palate at level of anteriormost premolar; 1, broad, wider than palate at anteriormost premolar (B55).

168. Width of maxilla compared to premaxilla (in middle of diastema): 0, maxilla as wide as premaxilla, 1, maxilla narrower than premaxilla, premaxilla is visible lateral to the maxilla in ventral view (B56).

169. Shape of premaxilla in ventral view: 0, sides almost parallel, snout tip slightly tapering; 1, snout tip tapering considerably; 2, sides parallel, snout tip with square-shaped appearance; 3, snout tip spoon shaped (B57).

170. Anterior expansion of medial postpalatal notch: 0, ends at the anterior half of M3 or further posterior; 1, extends to posterior end of M2 or further anterior (B58).

171. Shape of medial postpalatal notch: 0, rounded, parabolic to U-shaped; 1, pointy, V-shaped; 2, parabolic with distinct backward projection at the tip (B59).

172. Relative position of the medial and lateral postpalatal notches: 0, medial notch is always clearly posterior to the lateral notches; 1, medial notch more or less at the same level as lateral ones; 2, medial notch is always clearly anterior to lateral notches (B60).

173. Process of alisphenoid (anterior to foramen ovale): 0, barely developed or absent; 1, very prominent (B61).

174. Processus mastoideus (paroccipital process/processus paracondylaris), shape: 0, relatively broad, sometimes triangular; 1, very narrow (B63).

175. Mastoids and parietals: 0, far apart, never in contact; 1, relatively close, sometimes in contact; 2, very close, usually in contact (B64).

176. Ventral inflation of the tympanic bulla: 0, absent, ventral edge of bulla dorsal to ventral edge of occipital condyles; 1, intermediate, edge of bulla same at same level as occipital condyles; 2, strong, ventral edge of bulla ventral to occipital condyles (B65).

177. Tympanohyal vagina completely surrounded by inflated bulla: 0, no; 1, yes (B66).

178. Lamina vaginalis connected to opening of external auditory meatus, forming a "curtain" under it: 0, absent; 1, present (B67).

179. Shape of tympanic bulla in lateral view: 0, convex, half circle shaped or slightly flattened; 1, triangular, curving down posteriorly, with process adjacent to the mastoid process (B68).

180. Shape of tympanic bulla in ventral view: 0, spherical, length/width <1.66; 1, slightly elongate, length/width 1.67–1.85; 2, elongate, length/width 1.85–1.95; 3, very elongate, length/width >1.96 (B69).

181. Distinct basal process of tympanic bulla directly adjacent to basioccipital: 0, absent; 1, present (B70).

182. Bones contributing to the opening of the external auditory meatus: 0, bony rim formed by ectotympanic and squamosal (only half circle formed by ectotympanic); 1, bony rim (almost) entirely formed by ectotympanic (B71).

183. Orientation of external auditory meatus opening in ventral view: 0, directed laterally, 1, directed posteriorly (B72).

184. Position of external auditory meatus opening in lateral view (teeth orientated horizontally): 0, below or at the level of the mandibular fossa; 1, at least in part or completely above mandibular fossa (B73).

185. Rings on horn surface: 0, surface smooth/no rings; 1, prominent rings (B75).

186. Ring prominence: 0, prominent around entire horn (relatively equal on back and front); 1, no ring at back, or much flatter (B76).

187. Horn position in lateral view: 0, center of horn above posterior margin of orbit, some of the horn above orbit; 1, center of horn completely behind orbits (B78).

188. Horn position in frontal view: 0, very close together; 1, base situated at same distance to midline of skull and lateral edges of orbits; 2, far apart (B79).

189. Length of male horns (measured with a tape measure along the front line of the horn) as % of skull length (condyle-basal length): 0, very short, 75% or less; 1, short, 76%–120%; 2, intermediate 121%–175%; 3, long, 176%–240%; 4, very long, more than 250% (B80).

190. Horn core torsion: 0, no torsion; 1, right horn clockwise torsion (dorsal view, moving from base to tip); 2, right horn anticlockwise torsion (dorsal view, moving from base to tip) (B82, G13, G14, T15 & 16; G13/T15 state 1 coded as state 1, G14/T16 state 1 coded as state 2; state 0 is the same across all sources).

191. Degree of horn core torsion: 0, less than one full turn; 1, one full turn or more (B83).

192. Length of male horn core in relation to total length of skull: 0, short, horn-core length much shorter than skull length; 1, medium, horn-core length 85%–150% of skull length; 2, large, horn-core length >150% of skull length (B84).

193. Orientation of horn cores in frontal view (from base to tip): 0, parallel; 1, divergent; 2, only slightly divergent at the base, but greatly divergent towards the tips; 3, lyriform, parallel or slightly divergent at the base, but convergent towards the tips; 4, very divergent at the base, parallel or convergent towards the tips (B86).

194. Insertion angle of pedicle relative to tooth row: 0, <40°; 1, 40°–60°; 2, >60° (B87).

195. Curvature of horn core in lateral view: 0, straight or very little curved; 1, curved forward; 2, sinusoid, curved backward at the base and forward toward the tip; 3, curved backward (B88).

196. Direction of horn core compression: 0, no compression; 1, mediolateral; 2, anteroposterior (new composite character based on G2, G3, T4, T5, B81).



All issues of *Novitates* and *Bulletin* are available on the web (<http://digitallibrary.amnh.org/dspace>). Order printed copies on the web from:

<http://shop.amnh.org/a701/shop-by-category/books/scientific-publications.html>

or via standard mail from:

American Museum of Natural History—Scientific Publications  
Central Park West at 79th Street  
New York, NY 10024

∞ This paper meets the requirements of ANSI/NISO Z39.48-1992 (permanence of paper).